Politecnico di Torino

Politecnico di Torino

A.a. 2024/2025

Graduation Session December 2025

Optimization and validation of a wearable-based method for the ecological estimation of base of support parameters in healthy subjects

Supervisors:

Prof. Andrea Cereatti

Dr. Rachele Rossanigo

Dr. Marco Caruso

Candidates:

Giulia Cicalò

Acknowledgements

Con questo lavoro si conclude il mio percorso universitario, un cammino fatto di alti e bassi, di momenti entusiasmanti e altri più impegnativi. Non sarei mai riuscita a portarlo a termine senza alcune persone che oggi sento il dovere e il desiderio di ringraziare.

È doveroso da parte mia ringraziare il Professor Andrea Cereatti, Rachele e Marco per l'opportunità che mi è stata offerta: grazie per avermi permesso di approfondire un argomento a cui tenevo particolarmente, per aver contribuito alla mia crescita professionale e per avermi accompagnata, passo dopo passo, durante tutto il percorso.

Un grazie speciale alla mia famiglia, che mi ha sempre sostenuta moralmente ed economicamente, spronandomi a non arrendermi nei momenti più difficili. A voi devo tutto.

Ringrazio di cuore anche le mie amiche di sempre, che hanno creduto in me e mi hanno incoraggiata a dare sempre il massimo. La distanza non ci ha mai divise e mai ci dividerà.

Un pensiero ai miei colleghi: insieme abbiamo affrontato mille progetti, condiviso sfide, risate, chiacchiere e qualche spritz di troppo. Non avrei potuto desiderare compagni di viaggio migliori. Vi porto nel cuore.

Infine, ci tengo a ringraziare la mia famiglia allargata — cugini, cugine, zie e zii — a cui sono molto legata. Grazie per l'affetto che mi avete sempre dimostrato e per aver contribuito, ognuno a suo modo, a rendermi la persona che sono oggi.

Table of Contents

List of Figures

Abstract

Gait stability plays a crucial role in maintaining mobility and preventing falls, particularly among older adults and individuals affected by neurological disorders such as Parkinson's disease, multiple sclerosis, and dementia. Falls represent one of the leading causes of injury and loss of independence in these populations, highlighting the need for objective tools capable of identifying early markers of instability. Among the numerous parameters that describe human gait, stride width and step length—which together define the base of support—are considered fundamental indicators of postural control and balance. Variations in these parameters have been associated with altered motor strategies, compensatory mechanisms, and increased fall risk.

Traditionally, the assessment of base of support parameters has relied on laboratory-based motion capture systems, which provide highly accurate kinematic data but are limited by high costs, complex setups, and restricted ecological validity. In recent years, wearable technologies have emerged as a promising alternative, allowing gait to be analyzed in more naturalistic environments and across longer periods. Among these, inertial measurement units (IMUs) have gained particular relevance due to their portability, low cost, and ability to capture detailed spatiotemporal characteristics of walking.

Several studies have proposed methods to estimate stride width and step length using IMU data, sometimes combined with auxiliary sensors or machine learning approaches. These methods have shown promising results during straight walking, but their validation has rarely been extended to more complex gait conditions such as curvilinear trajectories, turning maneuvers, or simulated daily-life activities—contexts in which instability often emerges. Therefore, developing wearable-based methods that remain accurate across a variety of real-world walking conditions is an essential step toward the reliable assessment of gait stability.

Thesis overview

This thesis focuses on the development and validation of two methods for estimating base of support parameters using wearable sensors. The first is an optimized version of the approach proposed by Rossanigo et al. (2023), which combines IMU data with infrared Time-of-Flight (ToF) sensors to estimate the relative position of the feet. The second is the open-source method proposed by Wang et al. (2024), which relies exclusively on IMU data and machine learning techniques and, to the best of the author's knowledge, represents the only fully open-source implementation currently available in the literature.
Both methods were validated against a stereo-photogrammetric system during multiple walking conditions, including straight and curvilinear walking at three self-selected speeds, the Timed Up and Go (TUG) test, the 2-minute walking test, hallway walking, the 30-second sit-to-stand test, and simulated daily-life activities. Participants were equipped with four IMUs—two placed on the feet, one on the pelvis, and one on the head. The right-foot IMU was mounted on a rigid support hosting the ToF sensors, designed to detect the contralateral foot during the swing phase.
The optimization and validation of these methods aim to advance the field of wearable gait analysis by providing reliable tools for estimating stride width and step length in real-world conditions. Such approaches could support clinicians and researchers in the early detection of gait instability, enabling continuous and ecological monitoring of motor function in both healthy and pathological populations.

Chapter 1

State of the art: biomechanics and technologies for human gait analysis

The study of human gait represents a central topic in biomechanics, rehabilitation, and movement sciences, providing essential insight into how the neuromusculoskeletal system coordinates locomotion. Understanding gait is crucial not only for describing normal motor function but also for identifying alterations associated with neurological or musculoskeletal disorders. This chapter provides a comprehensive overview of the biomechanical and technological foundations of human gait analysis. The first section introduces the fundamental principles of gait biomechanics, outlining the main phases of the gait cycle and the principal spatiotemporal parameters that characterize human locomotion. The second part focuses on the evolution of measurement technologies, beginning with stereophotogrammetry, the recognized gold standard for motion capture, followed by the description of wearable systems based on magneto-inertial sensors and other alternative measurement devices. Finally, the chapter discusses the recent integration of machine learning approaches for the estimation of gait parameters, highlighting how data-driven methods are increasingly complementing traditional biomechanical analyses.

1.1 Human gait: biomechanical and clinical aspects

Human gait represents a fundamental motor activity characterized by complex interactions between the musculoskeletal system, the central and peripheral nervous systems, and sensory feedback mechanisms. Biomechanically, gait is defined as a cyclic and rhythmic process enabling the body to move forward efficiently while maintaining balance and stability [1]. The uniqueness of human gait lies in its stability, energy efficiency, and ability to adapt to various environmental and physiological conditions. The locomotor system is composed of skeletal frameworks, joints, muscles, tendons, and neural control pathways that, together, allow for movement generation and control, force transmission, and posture regulation. During walking, each lower limb alternately functions as a mobile lever and a load-bearing structure, enabling propulsion and support.
Although a healthy gait pattern is typically efficient, symmetrical, and energy-conserving, various neurological or musculoskeletal conditions can disrupt its structure and coordination. These disruptions are not merely mechanical; they often reflect underlying pathophysiological processes affecting central or peripheral motor pathways. Globally, millions of individuals experience gait abnormalities due to chronic or acute conditions [2].
Among these, *stroke* is particularly prominent as a cause of long-term disability. Depending on the location and severity of the brain lesion, stroke survivors may experience deficits ranging from mild limb incoordination to profound hemiparesis. These motor consequences often manifest as slowed, asymmetrical, and energy-inefficient gait, with poor postural control and limited adaptability [3] [4].
Parkinson's disease (PD) also profoundly affects gait, even in its early stages. Typical characteristics include reduced stride and step length, decreased walking velocity, diminished sagittal range of motion in lower limb joints, and increased double support time. As the disease progresses, gait becomes slower, less rhythmic, and more variable, with shuffling steps and festination being common [5] [6] [7]. These features reflect the underlying basal ganglia dysfunction and bradykinesia that impair motor amplitude regulation and adaptability, significantly increasing the risk of falls and loss of independence.
The prevalence and consequences of such impairments are not marginal. A significant portion of the global population lives with some form of disability affecting movement, and in many cases, the ability to walk safely and independently becomes compromised. This not only reduces mobility but also impacts broader aspects of life, including mental health, social integration, and quality of life, since walking is the most common form of locomotion involved in all activities of daily living [8].
For all these reasons the analysis of human gait is clinically relevant and it refers

to the systematic study of walking patterns, aiming to quantify and interpret the biomechanical, kinematic, and kinetic parameters that characterize locomotion. This discipline integrates knowledge from biomechanics, neuroscience, rehabilitation sciences, and engineering to evaluate how the human body generates and controls movement [9]. Gait analysis can be performed through observational methods, instrumented systems such as stereophotogrammetry, force platforms, and wearable sensors, each offering distinct advantages in capturing spatial-temporal parameters, joint angles, ground reaction forces, and muscle activation patterns [10].
The importance of gait analysis extends across multiple domains. Clinically, it provides an objective basis for diagnosing locomotor impairments, monitoring disease progression, and evaluating the effectiveness of therapeutic interventions [11]. In research, it serves as a key tool for understanding the underlying mechanisms of human locomotion and for developing advanced rehabilitation strategies. In sports science, gait analysis contributes to performance optimization and injury prevention.
Impairments in gait, whether due to neurological conditions, musculoskeletal injuries, or age-related decline, can significantly reduce independence, increase fall risk, and lower quality of life [12]. By enabling early detection of abnormal gait patterns, quantitative gait analysis supports timely interventions that can mitigate disability and improve long-term functional outcomes.
Given its relevance in both clinical and research contexts, understanding gait requires a detailed description of its fundamental structure. This begins with the concept of the *gait cycle*, the basic unit of locomotion, which describes the sequence of movements occurring between two consecutive contacts of the same foot with the ground.

1.1.1 The gait cycle

The gait cycle represents the fundamental unit of human walking, defined as the sequence of movements that occur between two consecutive initial contacts of the same foot with the ground [1]. It is a cyclic process that ensures forward progression while maintaining postural stability and energy efficiency. Understanding the gait cycle is essential for both clinical assessment and biomechanical research, as it allows for the identification of deviations from normative patterns and the quantification of locomotor performance.
The gait cycle is divided into two principal phases. The *stance phase* corresponds to the entire period of time during which the foot is in contact with the ground; it starts with an initial contact (heel strike) and ends with a final contact (toe-off) of the same limb. The *swing phase* corresponds to the period of time when the foot is in the air, moving forward preparing for the next contact, with all body weight transferred to the opposite foot, which is in the stance phase. This phase begins

with toe-off and ends with the next initial contact of the same foot. The stance phase accounts for approximately 60% of the gait cycle, while the swing phase accounts for the remaining 40Generally, each phase of the gait cycle is divided into sub-phases: five during the stance phase and three during the swing phase. The phases of the gait cycle are listed below with their respective percentages.
The stance phase is divided into:

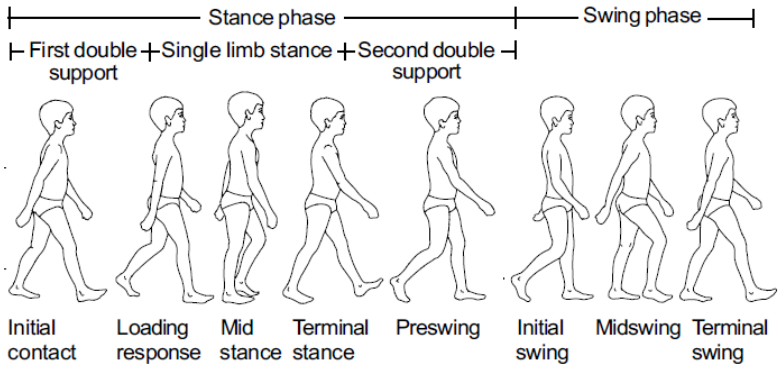

Figure 1.1: Gait cycle phases. Picture taken from [2]

1. *Initial contact (0%)*: the moment when the foot makes contact with the ground, also known as heel strike (HS).

2. *Loading response (0-10%)*: the beginning of the double support period, when the limb begins to accept weight. The body weight is transferred onto the leading limb, with shock absorption primarily provided by the knee flexors and ankle plantar flexors.

3. *Mid-stance (10-30%)*: first phase of single support when the body's center of mass passes over the supporting foot.

4. *Terminal Stance (30-50%)*: the heel lifts off the ground while the forefoot remains in contact, preparing for propulsion. It's the last phase of the single support ending with opposite initial contact.

5. *Pre-swing (50-60%)*: the knee flexes in preparation for swing and the body weight is transferred to the contralateral limb as the toes of the reference limb push off the ground.

The swing phase includes four sub-phases:

1. *Initial Swing (60-73%)*: it's the first third of the swing phase in which the foot leaves the ground, and the hip, knee, and ankle flex, with the ankle showing a

slight dorsiflexion. The leg begins to move forward in preparation for the next step.

2. *Mid Swing (73-87%)*: it's the middle third of the swing phase in which the limb swings beneath the body, with maximal knee flexion to ensure ground clearance.

3. *Terminal Swing (87-100%)*: it's the last third of the swing phase in which the knee extends, and the limb is properly positioned for weight acceptance. This sub-phase marks the end of the current gait cycle and the start of a new one.

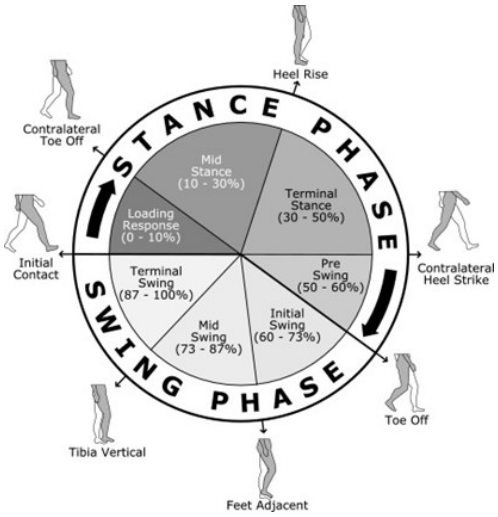

Figure 1.2: Gait cycle phases with all the events. Picture taken from [2]

There are seven events that divide the cycle of the step into the eight sub-phases described above.

- Initial contact (heel strike): the moment the heel first makes contact with the ground. It's the start event of the gait cycle.
- Contralateral toe-off: the toes of the contralateral foot push off the ground. This event divides the loading response phase from the mid-stance phase.
- Heel rise (heel off): the heel of the stance foot starts to rise away from the floor. This event divides the mid-stance phase from the terminal stance phase.
- Contralateral heel strike: the heel of the other foot touches down on the ground. This event divides the terminal stance phase from the pre-swing phase.

- Toe-off: the moment the toes leave the surface, ending contact with the ground. This event divides the pre-swing phase from the initial swing phase.

- Feet adjacent: the swinging leg passes alongside the stance leg during the forward motion. This event divides the initial swing phase from the mid-swing phase.

- Tibia vertical: the swinging leg's tibia aligns vertically with respect to the ground. This event divides the mid-swing phase from the terminal swing phase.

1.1.2 Description of principal spatio-temporal parameters of human gait

Spatio-temporal parameters represent the most fundamental descriptors of human gait, as they integrate both spatial (distance-based) and temporal (time-based) characteristics of locomotion. Unlike purely kinematic variables, which describe joint motion in terms of angular displacement, velocity, and acceleration, spatiotemporal parameters provide a macroscopic yet clinically meaningful view of walking performance [1] [9]. These measures are straightforward to obtain, reproducible across different populations, and highly sensitive to pathological alterations. Clinically, spatiotemporal analysis is employed to evaluate functional independence, detect gait asymmetries, and quantify fall risk, particularly in elderly or neurologically impaired populations.
The main spatio-temporal parameters of gait are describted below. [13]
The principal spatial parameters are:

- *Step Length*: the linear distance between the heel strike of one foot and the subsequent heel strike of the contralateral foot along the direction of progression. It reflects forward progression symmetry and is reduced in pathological or age-related gait.

- *Stride Length*: the distance between two consecutive heel strikes of the same foot along the direction of progression. It corresponds to two steps and serves as an indicator of overall gait efficiency.

- *Stride Width*: the mediolateral distance between the heel center of one footprint and the line of progression generated by two consecutive steps of the opposite limb. This parameter reflects the base of support and is strongly associated with gait stability.

Temporal parameters include:

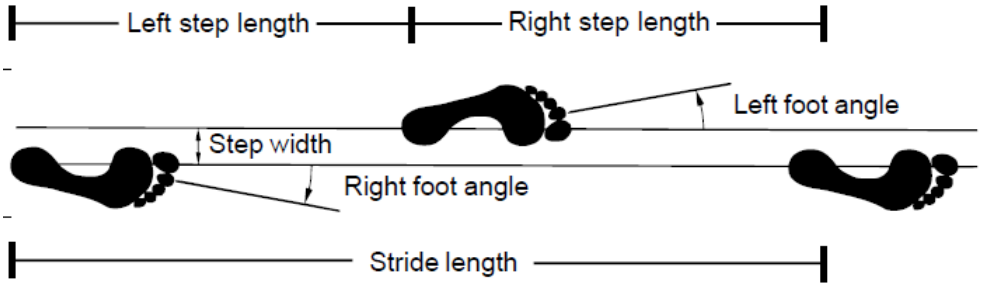

Figure 1.3: Spatial parameters of human gait. Picture taken from [14]

- *Stance Time*: the duration from heel strike to toe-off of the same foot, encompassing single and double support phases. Stance time is the interval during which the foot remains in contact with the ground. Prolonged stance times may indicate cautious gait patterns.

- *Swing Time*: the temporal interval between toe-off and the subsequent heel strike of the same foot, It quantifies the temporal duration of the non-weight-bearing phase during which the limb advances forward.

- *Step Time*: the temporal interval between the initial contact of one foot and the subsequent initial contact of the opposite foot.

- *Stride Time*: the elapsed time between two consecutive initial contacts of the same foot, representing the duration of a full gait cycle.

- *Single Support Time*: the period when only one limb is in contact with the ground, measured from the final contact of the contralateral limb to the next initial contact of the same contralateral foot. This parameter reflects dynamic stability during locomotion.

- *Double Support Time*: the proportion of the gait cycle where both feet are simultaneously in contact with the ground. Increased double support is typically associated with impaired stability.

- *Cadence*: the number of steps taken per minute, a measure of gait rhythm and efficiency. Normal adult cadence typically ranges from 100 to 120 steps/min.

- *Walking Speed (Velocity)*: average forward displacement of the body per unit of time, usually expressed in m/s. It results from the product of cadence and step length and is considered the most comprehensive measure of gait function.

1.2 Gait analysis technologies

The quantitative assessment of human gait requires dedicated instrumentation capable of capturing both kinematic and kinetic information during locomotion. Over the past decades, several technological approaches have been developed, ranging from laboratory-based optical motion capture systems, considered the gold standard in research, to portable and wearable sensors that allow for real-world monitoring of locomotor function. These technologies differ in terms of accuracy, portability, cost, and applicability, making their selection highly dependent on the clinical or research context [10] [11].
Broadly, gait analysis tools can be divided into two main categories:

- Non-wearable systems (laboratory-based): these include stereophotogrammetric optical systems for 3D motion capture, often combined with force platforms and electromyography (EMG) to obtain comprehensive biomechanical data. They provide high accuracy and reliability but are expensive, require controlled environments, and demand skilled personnel for data acquisition and processing [15].

- Wearable systems: these consist primarily of inertial measurement units (IMUs), accelerometers, gyroscopes, magnetometers, and pressure-sensitive insoles. They allow gait to be monitored outside the laboratory in natural environments, enabling long-term and ecological data collection. Despite their lower spatial resolution compared to optical systems, wearable sensors are increasingly adopted for clinical and rehabilitation purposes due to their portability and reduced cost [16].

In clinical and research applications, the integration of both technologies is becoming increasingly common, with hybrid systems offering complementary advantages: optical motion capture ensures high precision, while wearable sensors extend measurement capacity beyond the laboratory setting.
Stereophotogrammetry and magneto-inertial measurement units are described in detail below, as both were used in this work thesis.

1.2.1 Refernce system

Stereophotogrammetry represents the current gold standard for three-dimensional gait analysis due to its high spatial and temporal resolution, which allows precise reconstruction of human motion. These systems rely on multiple infrared cameras that track the position of reflective markers placed on specific anatomical landmarks according to standardized protocols (e.g., Plug-in Gait, Helen Hayes) [15] [10]. By capturing marker trajectories at high frame rates (typically 100–250 Hz), stereophotogrammetric systems can quantify joint kinematics, segmental displacements, and

angular velocities with sub-millimeter accuracy.
A typical stereophotogrammetric gait analysis system is composed of the following components:

- Infrared cameras: high-speed cameras positioned around the capture volume detect passive reflective markers placed on the body. Multiple cameras are used to ensure triangulation of marker positions for 3D reconstruction.
- Reflective markers: small spheres coated with retro-reflective material, attached to anatomical landmarks on the body. Their placement follows standardized protocols to accurately represent body segments and joint centers.
- Calibration tools: devices such as calibration wands or frames are used to define the coordinate system and to calibrate the cameras, ensuring accurate 3D reconstruction.
- Force platforms: embedded in the laboratory floor to measure ground reaction forces (GRFs) and moments, which are essential for kinetic analysis.
- Data acquisition workstation: a computer system running specialized software that collects, synchronizes, and processes marker trajectories and force data.
- Optional modules: Additional components may include surface electromyography (sEMG) for muscle activity recording and pressure-sensitive insoles for plantar pressure mapping.

Through the integration of these components, the system enables precise capture of human movement, providing the necessary data for both kinematic and kinetic analyses.
Stereophotogrammetric systems utilize *triangulation algorithms* to determine the 3D coordinates of each marker from the 2D images acquired by the cameras. The kinematic chain of the lower limbs is reconstructed by linking the markers through anatomical models, enabling the calculation of joint angles in three orthogonal planes:

- Sagittal plane: flexion-extension movements of the hip, knee, and ankle.
- Frontal plane: abduction-adduction and lateral tilt.
- Transverse plane: internal-external rotation of the joints.

The system's accuracy depends on careful marker placement, calibration of cameras, and subject preparation, as even minor marker misplacement can introduce errors in joint angle estimation [15].
Through the inverse dynamics approach, joint moments, powers, and reaction forces

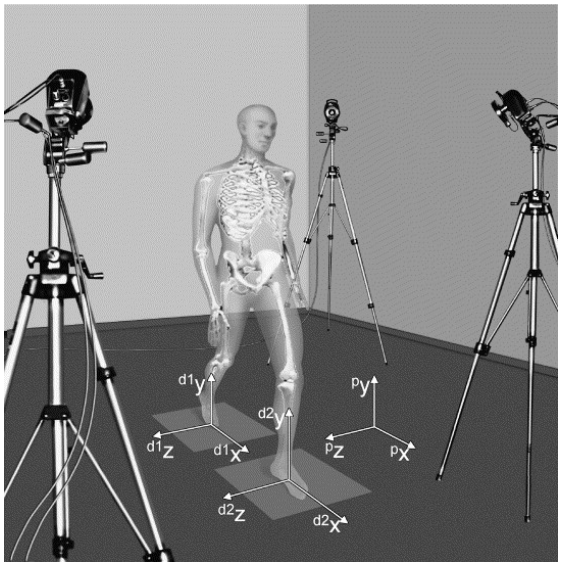

Figure 1.4: Typical instrumentation of a human movement analysis laboratory, featuring a stereophotogrammetry system and force plates embedded in the floor. Picture taken from [15]

can be estimated, linking the measured kinematics to the underlying forces and torques acting on the musculoskeletal system [9].
Stereophotogrammety ensures high spatial and temporal resolution, allowing accurate 3D reconstruction of complex movements, provides comprehensive kinematic and kinetic data, enabling detailed analysis of joint mechanics and serves as a validation reference for novel wearable and markerless systems. However, the stereophotogrammetric system also has some limitations:

- Requires controlled laboratory conditions, limiting ecological validity.
- High cost and technical complexity of setup, calibration, and data processing.
- Short measurement distances, which may not capture natural gait patterns during long or outdoor walking.
- Dependence on skilled operators for accurate marker placement and data interpretation.

Despite limitations, stereophotogrammetry is extensively used in many applications: clinical gait assessment for neurological, orthopedic, and pediatric populations. rehabilitation monitoring to evaluate treatment outcomes, research for validating new gait analysis technologies, including wearable sensors and markerless motion capture systems.

In summary, stereophotogrammetry remains the benchmark technique for precise, high-resolution gait analysis. Its combination with force measurement and EMG provides unparalleled insights into human locomotion biomechanics, making it indispensable for both clinical and research applications [10][15] [17].

However, while stereophotogrammetry excels in capturing detailed kinematic and kinetic data, it requires specialized laboratories, extensive setup, and expertise, which can limit its routine clinical use. For more accessible assessment of spatiotemporal gait parameters, systems like GAITRite offer a practical alternative. GAITRite is an electronic walkway embedding a dense matrix of pressure-activated sensors within a portable carpet. As a subject traverses the active area, heel-strike and toe-off events are detected from spatiotemporal patterns of sensor activations. From these events, the system computes temporal (step/stride time, stance/swing time, single/double support) and spatial parameters (step/stride length, step width, foot progression angle, base of support). Typical research-grade configurations feature an active area on the order of 4.9 m $\times$ 0.61 m with sampling around 120 Hz, enabling multiple consecutive steps with millisecond timing precision in clinical corridors or labs [18].
Multiple studies have established strong test–retest reliability and concurrent validity of GAITRite for most spatiotemporal metrics in healthy adults and older populations. In seminal work, Bilney et al. and Menz et al. reported excellent reliability/validity for step time, stride time, cadence, and velocity; they cautioned that base of support and foot progression angles show higher coefficients of variation, warranting care in clinical interpretation. Subsequent investigations and systematic comparisons confirm GAITRite as a reference platform for temporal–spatial gait outcomes [19].
GAITRite has many pros and cons: strengths include standardized, low-burden setup; direct footprint mapping with robust event detection and strong repeatability across sessions. Limitations are inherent to walkway length just a few steps are allowed, which constrains steady-state steps and ecological validity, and continuous daily-life monitoring is not feasible. Despite of its limitations, GAITRite is often used as a benchmark for validating newer wearable systems. [18][20]

Figure 1.5: Illustration of a GaitRite pathway. Picture taken from [21]

1.2.2 Wearable technology: the Magneto-Inertial Measurement Units

In the last two decades, Magnet-Inertial Measurement Units (MIMUs) have become increasingly widespread in gait analysis and human movement science. Their success is due to the evolution of MEMS technology (Micro-Electro-Mechanical Systems), which allows the miniaturization of sensing elements at extremely low cost and energy consumption, making them suitable for wearable applications [22]. Unlike stereophotogrammetric systems, which are confined to laboratory environments, MIMUs provide the opportunity to study locomotion in ecological conditions, over long durations, and across many contexts ranging from clinical monitoring to sports performance.
A standard MIMU integrates three types of sensors: accelerometers, gyroscopes, and magnetometers, each of them mounted on orthogonal axes, thereby forming a so-called 9-axis sensing device. In addition, modern MIMUs often include auxiliary components such as microcontrollers, pressure and temperature sensors, and wireless communication modules (e.g., Bluetooth) for real-time data transmission.
The combined use of these sensors allows reliable estimation of orientation, angular velocity, and linear acceleration through sensor fusion algorithms (e.g., Kalman filters), compensating for the individual limitations of each sensor. This integration has enabled MIMUs to emerge as a valid alternative to traditional gait analysis tools, particularly in applied and clinical domains.
The three types of sensors that make up a MIMU are described in detail below.

Accelerometer

The accelerometer represents the most fundamental sensing element, as it provides direct information on the linear accelerations experienced by the body segment to which it is attached. Its functioning relies on the principle of Newton's second law, whereby a small inertial mass, suspended within the sensor housing, resists changes in motion. The basic model is a mass-spring-damper system: a proof mass is suspended inside the sensor casing by elastic elements. When the sensor undergoes linear acceleration, inertia causes the mass to lag behind, deforming the spring. The displacement is proportional to the applied acceleration, which is then converted into an electrical signal.
Mathematically, the proof mass dynamics follow a second-order differential equation:

$$m\ddot{x} + c\dot{x} + kx = F(t) = ma \tag{1.1}$$

where m is the proof mass, k the spring stiffness, c the damping coefficient, and a the acceleration of the frame.

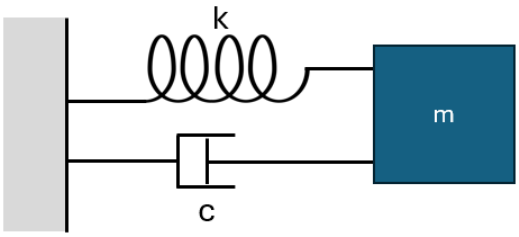

Figure 1.6: Schematic illustration of an accelerometer composed of a mass, spring, and damper

Different technologies exist for the transduction of this displacement.

- *Capacitive accelerometers*: displacement of the proof mass alters the distance between capacitor plates, producing measurable capacitance changes that can be converted into a voltage signal. Multiple plates increase sensitivity.
- *Piezoelectric accelerometers*: exploit the intrinsic property of certain crystals to generate surface charges when subjected to mechanical stress; the inertial mass compresses the crystal, and the resulting charge is directly proportional to the applied acceleration.

The signal measured by an accelerometer can be modeled as:

$$y(t) = a(t) - g(t) + n(t) \tag{1.2}$$

where g(t) is the gravitational acceleration and n(t) represents stochastic noise, including thermal noise, electronic noise, and quantization effects.
Each type has trade-offs: capacitive sensors are more suitable for low-frequency movements (e.g., gait), while piezoelectric sensors excel in capturing high-frequency events such as impacts.
Although accelerometers are widely employed in gait analysis due to their ability to capture linear accelerations, it is important to emphasize that they do not directly measure translational acceleration in an absolute sense.
Instead, they sense the so-called specific force, defined as the non-gravitational acceleration acting on the sensor [23]. Mathematically, this relationship can be expressed:

$$f = a - g \tag{1.3}$$

where f is the specific force measured by the accelerometer, a is the coordinate acceleration of the sensor and g is the gravitational acceleration vector.
This means that accelerometers inherently measure the combination of motion-induced acceleration and the gravitational component but cannot themselves distinguish between the two.
In static conditions, the coordinate acceleration is zero, so the accelerometer output reduces to:

$$f = -g \tag{1.4}$$

Thus, the accelerometer senses only gravitational acceleration, which is projected onto its three orthogonal measurement axes. In dynamic conditions, the coordinate acceleration is non-zero, so the output is the sum of both gravitational and coordinate acceleration. This makes it difficult to distinguish whether a signal results from a linear movement of the body or from a simple change in orientation with respect to gravity. For this reason, accelerometers are typically integrated with gyroscopes and magnetometers within a sensor fusion framework.

Gyroscope

While accelerometers provide access to translational dynamics, gyroscopes are indispensable for capturing the rotational behavior of body segments. A gyroscope does not directly measure orientation, but rather the instantaneous *angular velocity* vector ω of the sensor frame with respect to an inertial reference frame. The operating principle of modern MEMS gyroscopes relies on the Coriolis effect. In these devices, a microscopic proof mass is suspended within the sensor structure and is continuously driven into oscillation along a predetermined axis, conventionally referred to as the drive axis. Under stationary conditions, the oscillatory motion of the mass remains confined to this axis, and no displacement is registered in

orthogonal directions.
When the sensor undergoes a rotation around an axis perpendicular to the drive axis, the oscillating mass is subjected to the Coriolis force, which can be expressed as:

$$F_c = -2m(\omega \times v) \tag{1.5}$$

where m is the proof mass, v is its velocity along the drive axis, and ω denotes the angular velocity vector of the sensor. The Coriolis force induces a secondary oscillation along a direction orthogonal to both the drive axis and the axis of rotation, conventionally termed the sense axis. The displacement of the proof

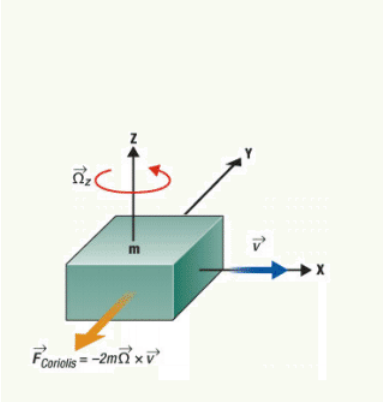

Figure 1.7: Schematic rappresentation of a gyroscope

mass along the sense axis is extremely small and requires precise transduction mechanisms for detection. MEMS gyroscopes generally employ:

- *Capacitive* transduction, whereby the displacement modifies the capacitance between electrodes, and the variation is converted into a voltage proportional to angular velocity.

- *Piezoelectric* transduction, in which mechanical stress applied to a piezoelectric element by the moving mass generates an electric charge.

In both cases, the amplitude of the sense-mode oscillation is directly proportional to the applied angular velocity, providing the gyroscope with its measurement capability [24].
The dynamics of the proof mass in the sense direction can be described by a second-order differential equation of the mass–spring–damper type:

$$m\ddot{x}_s + c_s\dot{x}_s + k_s x_s = 2m\omega x_d \tag{1.6}$$

where x_s is the displacement along the sense axis, c_s and k_s are the damping and stiffness coefficients, x_d is the velocity of the driven oscillation, and ω represents the applied angular velocity. When operated near the resonance frequency of the sense mode, the response x_s becomes highly sensitive to ω, thereby enhancing the sensor's performance [25].
The gyroscope output can be formally modeled as:

$$y(t) = \omega(t) + b(t) + n(t) \tag{1.7}$$

where $\omega(t)$ is the true angular velocity, $b(t)$ is a bias term and $n(t)$ represents stochastic noise. Thus, the output of a gyroscope, like the one of the accelerometers, is warped by the presence of bias and noise and this represents the main limitation: orientation estimates from gyroscopes alone diverge over time, necessitating correction through accelerometer and magnetometer fusion. Despite their susceptibility to drift, gyroscopes are indispensable in gait analysis, as they provide highly accurate measurements of rapid angular dynamics, such as joint rotations during swing and stance phases, which cannot be reliably captured by accelerometers alone.

Magnetometer

Magnetometers are sensors designed to measure the intensity and orientation of magnetic fields. Within MIMUs, they play a fundamental role by providing an absolute reference for orientation, in particular for the yaw (heading) angle, which cannot be resolved solely through accelerometers and gyroscopes [26] [22].
The principle of operation most commonly exploited in MEMS magnetometers is the Hall effect. When an electric current I flows through a thin conductive or semiconductive element of thickness d in the presence of a magnetic field B orthogonal to the current flow, the charge carriers (electrons or holes) experience a Lorentz force:

$$F_L = q(v \times B) \tag{1.8}$$

where q is the elementary charge and v the drift velocity of the carriers. The deflection of carriers leads to an accumulation of charges on the sides of the conductor, which generates a transverse voltage known as the Hall voltage:

$$V_H = \frac{IB}{nqd} \tag{1.9}$$

where n is the carrier density. The Hall voltage is directly proportional to the component of the magnetic field orthogonal to the current, and with appropriate orthogonal sensor axes, the full three-dimensional magnetic field vector can be reconstructed [25]. In inertial navigation, the magnetometer measurement can be

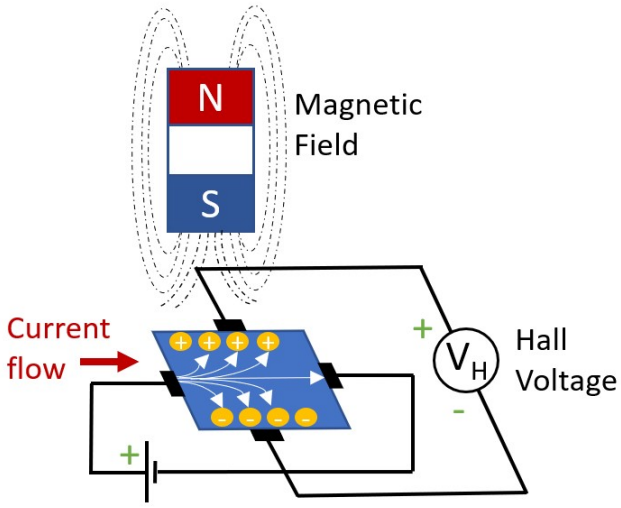

Figure 1.8: Schematic illustration of how a magnetometer work

expressed as:

$$m(t) = R(t)BE + n(t) \tag{1.10}$$

where $m(t)$ is the measured magnetic field in the sensor frame, $R(t)$ is the rotation matrix from the inertial to the sensor coordinate frame, BE is the Earth's magnetic field vector and $n(t)$ represents measurement noise and distortions.
In ideal conditions, magnetometer data provides a robust absolute reference for orientation, particularly valuable in correcting gyroscope drift within sensor fusion frameworks such as complementary filters and extended Kalman filters [26].
In practice, magnetometer measurements are significantly affected by environmental factors:

- Hard-iron distortions, caused by permanent magnetization of nearby ferromagnetic materials, shift the measured field vector.
- Soft-iron distortions, caused by ferromagnetic structures that locally deform the field lines, alter the apparent direction and magnitude of the field.
- Electromagnetic interference, arising from power lines, electronic devices, or medical equipment, introduces transient perturbations.

These distortions can compromise heading estimation and must be mitigated through calibration techniques such as ellipsoid fitting or online adaptive algorithms [27].
In gait analysis, magnetometers are especially valuable because they provide the

missing heading information, allowing a complete three-dimensional reconstruction of limb or trunk orientation when fused with accelerometer and gyroscope data. However, their reliability is environment-dependent: while outdoor measurements tend to be more stable, indoor environments rich in ferromagnetic materials (e.g., hospitals, laboratories, or gyms with metallic equipment) may generate distortions that limit their applicability.
The accelerometer, gyroscope, and magnetometer each have distinct strengths and limitations. Together, through sensor fusion, they provide a comprehensive and reliable characterization of human movement. Accelerometers capture translational dynamics but cannot discriminate tilt from translation; gyroscopes quantify angular velocity but suffer from drift; magnetometers offer absolute orientation but are sensitive to disturbances. The integration of the three within MIMUs explains their rapid expansion in gait analysis, clinical monitoring, and sports applications.

1.2.3 Alternative wearable tecnologies

Another wearable technology used in gait analysis are smart in-shoe systems, like *instrumented insoles*. These smart insoles integrate arrays of plantar pressure sensors capacitive, resistive or piezoresistive, and, in some models, embedded IMUs. They stream or log vertical load surrogates, regional pressure, center-of-pressure (COP) trajectories, and gait phase timing. Because they live inside the shoe, insoles enable free-living capture across terrains and sessions, complementing lab-based measures with ecologically valid data [28]. There are several types of smart insoles that have been clinically proven to be effective:

- *Loadsol* single-/multi-sensor wireless insoles have shown moderate-to-excellent validity (ICC typically 0.69–0.98) and improved performance at higher sampling (200 Hz), with small systematic underestimation of peak loads in some conditions and good symmetry metrics; independent studies against instrumented treadmills and Pedar have corroborated force-related validity in walking/running and even loaded marching [29] [30] [31].

- *Moticon OpenGo* multi-sensor insoles have been validated versus force plates and Pedar for discrete and time-normalized variables across walking, jumping, and balance tasks, supporting their use for spatiotemporal events and plantar loading patterns in ambulatory settings [28] [32].

- *PODOSmart* smart insoles, integrating inertial and pressure sensing, have demonstrated strong validity when compared with stereophotogrammetry-based motion capture. Validation studies reported high intraclass correlation coefficients (ICCs > 0.91) for cadence, walking speed, and step duration, and

acceptable-to-high agreement for spatial parameters such as stride length and foot progression angle. The system also showed excellent test–retest reliability across repeated measurements, confirming its robustness for gait parameter estimation [33].

Figure 1.9: Image of PODOsmart inslole system

Smart insoles provide dense step-by-step loading information and precise gait phase segmentation outside the lab; they are well-suited to longitudinal monitoring (rehabilitation, sports, frailty). Key caveats include sensor drift and hysteresis (especially with resistive elements), footwear fit effects, temperature/humidity influences, and occasional force-magnitude bias relative to force plates—effects that can be mitigated via per-session calibration and model-based corrections.

1.2.4 Instability monitoring and relevance of base of support parameters

Wearable technologies are widely used for monitoring gait stability, whose clinical relevance is well established, as gait instability is strongly associated with increased fall risk, particularly in older adults and individuals with neurological disorders [19]. Stability during walking reflects the ability to maintain the body's center of mass within the base of support, adjusting dynamically to internal and external perturbations [17]. Impairments in this ability can lead to unsteady gait, higher variability in step patterns, and an increased likelihood of trips or falls.

Among the parameters used to assess gait stability, base-of-support (BoS) metrics are particularly informative. The BoS represents the area enclosed by the points of contact between the feet and the ground at any given moment, providing a geometric boundary for balance [15]. Key BoS-related parameters include stride

width, defined as the lateral distance between consecutive footfalls of opposite feet; step length, the anteroposterior distance between consecutive foot contacts of the same foot; and the overall BoS area, which reflects the combined spatial extent of foot placement and serves as a proxy for lateral and forward–backward stability [19]. Variability in these parameters—such as changes in step length or fluctuations in stride width—has been linked to reduced postural control and increased fall risk, making them central metrics in clinical gait analysis and rehabilitation monitoring.

The clinical importance of accurately estimating stride width and step length lies in their direct association with balance control and fall risk. Step length reflects the anterior-posterior progression of gait and overall functional mobility, while stride width indicates mediolateral stability and the capacity to maintain postural control during walking. Changes in these parameters are commonly observed in older adults and in individuals with neurological disorders, such as Parkinson's disease, multiple sclerosis, and dementia, and are predictive of higher fall risk, reduced independence, and impaired daily functioning [5]. Reliable measurement of stride width and step length under real-world conditions can therefore provide clinicians with valuable tools for early detection of gait impairments, continuous monitoring of disease progression, and evaluation of interventions aimed at improving stability and preventing falls [19].

Despite their importance, standard MIMU-based systems, described above, cannot provide all the spatial information necessary to accurately estimate these BoS parameters, as inertial sensors alone do not directly capture the lateral distance between the feet or the precise geometric configuration of foot placement during stance. To overcome this limitation, additional sensing technologies must be integrated, enabling a more complete reconstruction of BoS metrics and a more reliable assessment of gait stability.

1.2.5 Base of support parameters estimation: deterministic vs machine learning approaches

To overcome the limitations of standalone MIMUs in estimating base-of-support (BoS) parameters, the literature describes two principal strategies: deterministic sensor-fusion approaches and machine-learning-based methods. Sensor fusion combines inertial measurements with complementary sensing technologies to reconstruct foot placement and BoS metrics with higher accuracy. Among these, Weenk et al. and Van Meulen et al. employed ultrasonic distance sensors integrated with foot-mounted IMUs [34] [35], while Hung et al. (2013) used camera-based optical distance sensors [36]. Backlund et al. (2019) and Rossanigo et al. (2023) adopted infrared distance sensors combined with foot-mounted IMUs to reliably estimate BoS parameters, including stride width and step length [37] [38]. These approaches exploit deterministic algorithms to integrate multiple sensor modalities, effectively

compensating for the spatial information that MIMUs alone cannot capture.
In parallel, machine learning (ML) has transformed gait analysis by enabling the estimation of BoS parameters directly from inertial signals, without requiring additional physical sensors. Different IMU configurations have been explored for this purpose. Zadka et al. and Hannink et al. demonstrated that a single IMU mounted on the lower back can provide sufficient signals to infer BoS parameters [39] [40], whereas Wang et al. employed a three-IMU setup (two foot-mounted and one pelvic-mounted) to estimate stride width with higher spatial fidelity [41]. More complex configurations have also been tested, including Renani et al.'s system with seventeen IMUs distributed across multiple body segments [42], and Vandermeeren et al.'s approach using a single smartphone as the inertial source [43].
In the present study, two representative methods were selected to illustrate each solution. For the machine-learning approach, Wang et al. [41] was chosen as it represents the only open-source framework currently available in the literature for stride width estimation, providing transparency and reproducibility. For the sensor-fusion approach, the method by Rossanigo et al. [38] was adopted, as it enables miniaturization of the sensors while maintaining accurate BoS reconstruction, and was developed within the research group where this thesis work was conducted. These selections allow a detailed analysis of both deterministic and data-driven approaches for BoS parameter estimation, providing a comprehensive foundation for subsequent stability assessment. Figure 1.10 provides a summary of the sensor-fusion methods, while Figure 1.11 illustrates the machine-learning-based approaches.

Author (year)	Setup	Parameter	Validation
Backlund T. et al. (2020)	2 IMU + 1 distance sensor	Stride width	Healthy and pathologic
Köse A. et al. (2012)	1 IMU	Step length	Healthy subjects
Rossanigo R. et al. (2023)	1 IMU + 2 distance sensor	Step length, stride width, area BoS	Healthy subjects
Vezočnik M. et al. (2022)	4 smartphone	Step length	Healthy subjects
Weenk D. et al. (2015)	IMU + ultrasound sensors	Step length, stride width	Healthy subjects

Figure 1.10: Summary of sensor fusion methods.

Author (year)	Setup	Parameter	Validation
Zadka A. et al (2024)	1 IMU	Step length	Healthy and pathologic
Stenger R.et al (2024)	1 IMU + GAITRite	Step length	Healthy subject
Verbiest J. R. et (2023)	1 IMU	Stride length	Healthy subjects
Wang H. et al. (2024)	3 IMU	Stride width	Healthy and pathologic
Hannik J. et al. (2017)	1 IMU + GAITRite	Stride length, Stride width	Patological subjects

Figure 1.11: Summary of machine learning methods.

Chapter 2

Materials and methods

As discussed in Chapter 1, a wide range of technologies and approaches have been developed for gait analysis, each with specific advantages and constraints. Building on this background, the present thesis focuses on the validation of an estimation method for key spatiotemporal parameters, with particular attention to stride width, step length, and the base of support area. In addition to comparisons with established reference systems, the method is also benchmarked against a machine learning model proposed in the literature. This chapter outlines the objectives of the thesis and provides a comprehensive description of the materials and methods used, including the participant cohort, experimental protocol, instrumentation, and statistical analysis framework.

2.1 Objectives of the thesis work

The main goal of this study was to optimize and validate a wearable-based method for the estimation of base of support (BoS) parameters, specifically stride width and step length, through the integration of inertial and infrared distance sensor. The study focused on extending and refining the approach proposed by Rossanigo et al. (2023), addressing its main limitations related to validation conditions restricted to straight walking, and limited signal preprocessing. The optimized method (M1) combined data from foot-mounted magneto-inertial measurement units (MIMUs) and infrared time-of-flight (ToF) sensors to provide accurate inter-foot distance estimates across both straight and curvilinear locomotion. The estimates of all parameters were validated by comparison with the gold standard method, stereophotogrammetry.

A secondary objective was to compare the performance of the proposed method

(M1) with a reference machine-learning model (M2) from the literature [41], representing an alternative data-driven approach to stride width estimation. This comparison aimed to assess the relative accuracy, robustness, and generalizability of a physics-based sensor-fusion framework versus an ML-based inference strategy.

Overall, the thesis sought to determine whether the optimized wearable configuration and processing pipeline could achieve reliable BoS parameter estimation under ecologically valid walking conditions, thereby supporting future applications in real-life monitoring of gait stability in both healthy and clinical populations.

2.2 Workflow of the implemented methods

2.2.1 Method by Rossanigo et al. 2023 (M1)

The method proposed by Rossanigo et al. (2023) (M1) utilizes a wearable system attached to a single foot, which was chosen to be the right one, to estimate spatio-temporal gait parameters. The right foot was instrumented with a magneto-inertial measurement unit (MIMU) and two infrared time-of-flight (ToF) distance sensors, all mounted on a custom 3D-printed rigid support.
The proposed workflow for Base of Support (BoS) parameters estimation is structured as a sequential five-step pipeline. Each step is illustrated with a corresponding image panel (Figure 2.1 to Figure 2.5) which visually clarify how each stage of the workflow was implemented.

1. *Pose and orientation estimation of the instrumented foot.*
   The pipeline begins with the estimation of the position and orientation of the instrumented (right) foot using the approach described by Salis et al. (insert full citation). This step provides the local foot reference frame and time-synchronized kinematic information that are used throughout the subsequent processing stages.

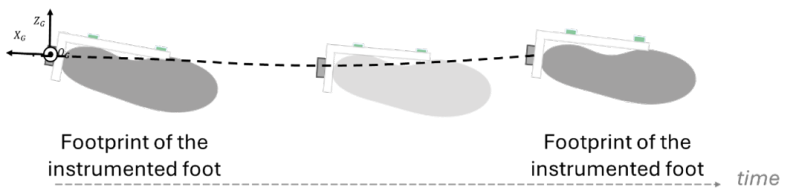

Figure 2.1: Step 1: Pose and orientation estimation of the instrumented foot

2. *Medial scan of the non-instrumented foot during stance.*
   While the instrumented foot is in swing, distance sensors mounted on it record

measurements of the medial side of the non-instrumented (left) foot during the latter's stance phase. These distance readings form a sparse spatial scan of the medial border of the contralateral foot.

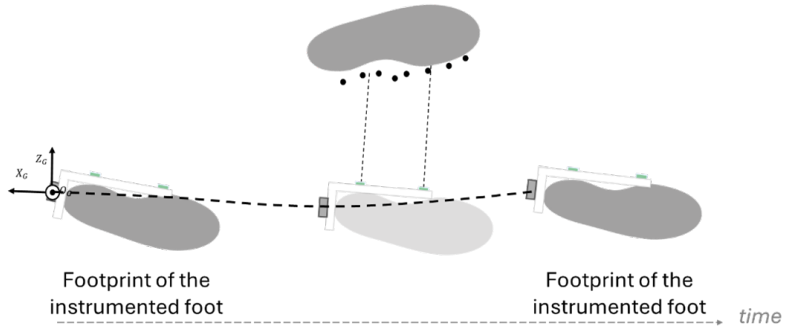

Figure 2.2: Step 2: Medial scan of the non-instrumented foot during stance

3. *Linear modelling of the medial foot border.*
   The acquired distance samples are used to fit a parametric (linear) model of the medial side of the non-instrumented foot. The linear fit approximates the medial contour in the local coordinate system and regularises sensor noise, producing an interpretable geometric representation suitable for footprint reconstruction.

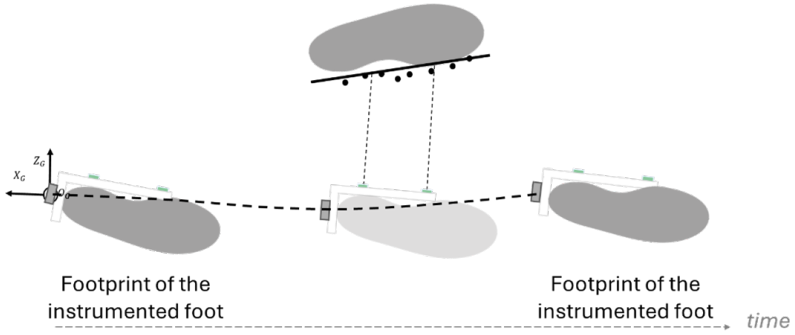

Figure 2.3: Step 3: Linear modelling of the medial foot border

4. *Estimation of consecutive footprints in a common reference frame.*
   Using the instrumented foot pose and the fitted medial model, consecutive footprints of both sides are reconstructed and expressed in the same global reference frame.

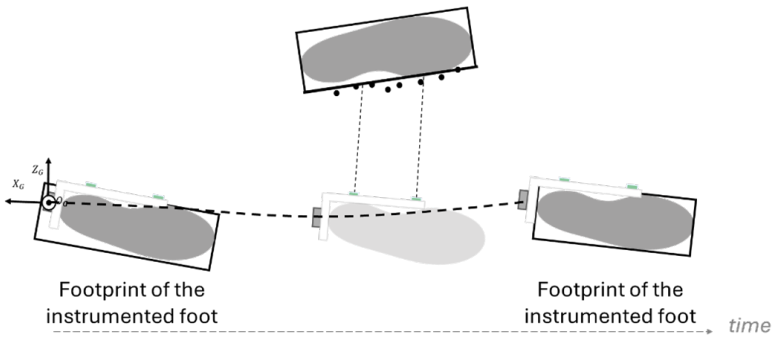

Figure 2.4: Step 4: Estimation of consecutive footprints in a common reference frame

5. *Computation of Base of Support (BoS) parameters.*
   With the reconstructed left and measured right footprints available in the common frame, BoS parameters (stride width, step length, and AreaBoS) are computed for each gait cycle and aggregated as needed. The procedure yields both the "right" and the "left" components of each parameter as well as combined measures.

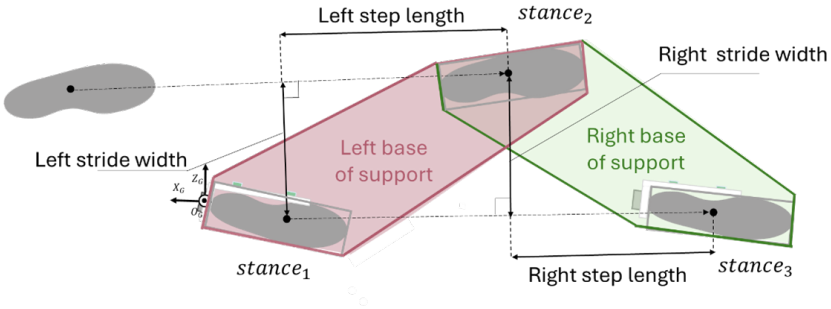

Figure 2.5: Step 5: Computation of Base of Support (BoS) parameters

An essential phase of this method was sensor calibration. The MIMU was calibrated using established procedures proposed by [44] [45] to minimize bias in the accelerometer, gyroscope, and magnetometer readings. The distance sensors were calibrated through a custom 3D-printed calibration device that imposed a known distance between each sensor and a reflective target, allowing offset estimation and compensation. This ensured consistent performance across subjects and trials.
While the work of Rossanigo et al. (2023)[38] demonstrated the feasibility and validity of this approach for out-of-laboratory gait analysis, a critical aspect was identified that limited the method's generalizability and applicability:

- Validation on straight-line walking only: the original validation was conducted on thirteen healthy adults walking along a 5-meter straight path. This narrow focus on linear locomotion does not account for the complexities of curvilinear walking or turning, which are common motor tasks in daily life.

To address these limitations, a series of methodological refinements have been implemented for the present study:

- Generalization of the Base of Support (BoS) definition: the definition of the BoS area has been generalized to be more universally applicable to complex walking scenarios. While Rossanigo et al. (2023) defined the BoS as a polygon between the rectangular footprints, this study aims to refine this definition to be more robust to changes in foot placement during non-linear tasks.

Another limitation of Rossanigo et al. work was the instrument bulkiness: despite being wearable, the 2023 prototype remained relatively cumbersome due to its cabling and rigid support, which made it impractical for use in populations with mobility impairments. Even for healthy participants, the system's size and positioning affected natural gait, indicating that further miniaturization and redesign are required for clinical or real-world deployment.
To improve comfort and wearability a new prototype was developed, making it suitable for both healthy and pathological subjects.
The 2023 prototypeshowed in Figure 2.6, presented by Rossanigo et al., included a rectangular rigid support ($155 \times 42 \times 22$ mm, 40 g) fixed on the medial side of the shoe with straps and cabled sensors, offering accurate performance but limited comfort.

Figure 2.6: Old setup used by Rossanigo et al.(2023)

The new configuration significantly reduces the system's overall bulk, weight, and wiring as shown in Figure 2.7 and aims to maintain the estimation accuracy of BoS-related parameters while achieving greater adaptability to different user populations, including those with pathological gait.
Since the new prototype introduced changes in the mechanical structure and

sensor layout compared to the 2023 design, the calibration procedure used by Rossanigo et al. (2023) was revised to adapt it to the new configuration and improve measurement reliability.

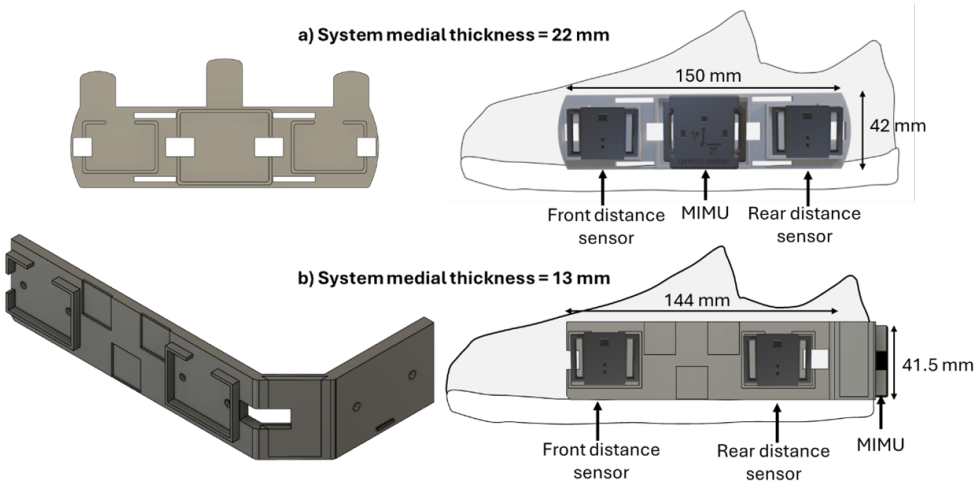

Figure 2.7: Comparison between new and old setup

2.2.2 Methodological refinements of M1: a new calibration and a personalization procedure

In the original work by Rossanigo et al. (2023), the calibration procedure was designed to align the coordinate system of the wearable module with the longitudinal axis of the foot and to ensure correct orientation of the distance sensors relative to the inertial unit. The procedure relied on a short static trial (approximately 10 seconds) during which the subject remained still. During this phase, the mean accelerometer, gyroscope, and magnetometer signals were used to determine the MIMU orientation, while the distance sensor readings were averaged to compute the calibration angle (α_{calib}). Figure 2.8 shows the calibration angle.

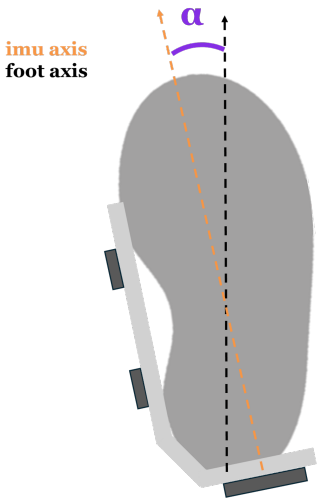

Figure 2.8: Rappresentation of the calibration angle

The relative positions of the two distance sensors (rear and front) were used to define the longitudinal alignment of the rigid support with respect to the MIMU coordinate system, according to the following steps:

1. Extraction of raw accelerometer, gyroscope, and magnetometer data during the static phase.

2. Orientation estimation through a Madgwick filter to obtain the mean quaternion describing the rigid support pose.

3. Projection of the two distance sensor position vectors in the MIMU reference frame.

4. Calculation of the calibration angle (α_{calib}) as the angle between the line connecting the two sensors and the anteroposterior axis of the MIMU.

5. Definition of the rotation matrix R_{calib} applied to all subsequent data to ensure proper alignment of the sensors with the foot axis.

The new configuration improved compactness and wearability but required a more refined calibration to correct for small geometric deflections of the support and for intrinsic offsets of the distance sensors.
The updated calibration method therefore introduces several key modifications:

1. Sensor-specific calibration parameters:
   Each ToF sensor is characterized by a linear calibration model (slope and offset) determined from pre-acquisition calibration routines and stored in a

system's data. Calibrated readings were adjusted using these parameters in order to restore the original raw readings, as the applied calibration was found to be unsuitable.

2. Offset compensation at 10 cm reference distance:
   Empirical offsets estimated during preliminary tests are applied to compensate for sensor-dependent bias at a known reference distance, ensuring consistency between front and rear sensor readings.

3. Deflection correction and shift compensation:
   To account for possible slight bending of the support or positioning asymmetries, two additional parameters are introduced:

   - β_{defl}: is the deflection angle
   - β_{shift} it represents the linear displacement induced by the deflection of the front sensor with respect to the rear sensor.

   These parameters are used to geometrically correct the front sensor reading through a cosine transformation and a linear shift term, effectively modeling the small rotation and translation between sensors. They were calculated using Geogebra software as shown in Figure 2.9.

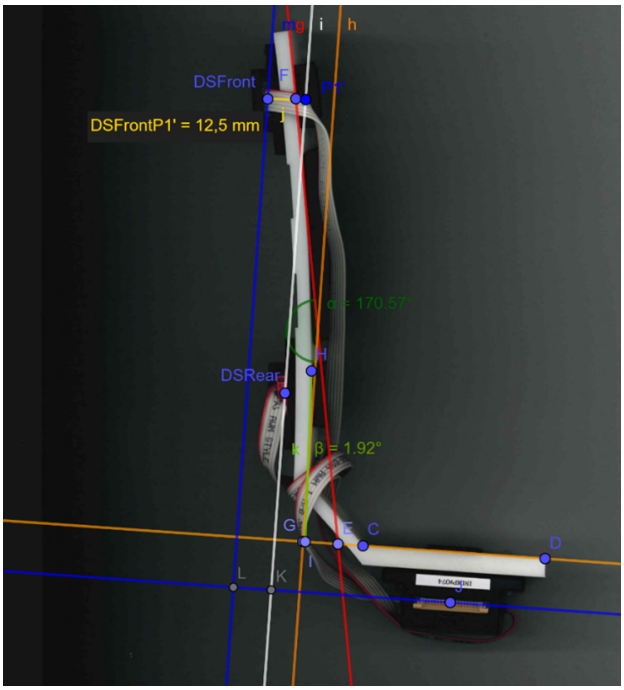

Figure 2.9: Estimation of β_{defl} and β_{shift} by Geogebra

4. Geometric computation of the calibration angle ($\alpha_c alib$): Using the corrected rear and front sensor distances and the fixed inter-sensor distance measured with Geogebra, the calibration angle is computed using the arctangent relationship:

$$\alpha_{\text{calib}} = \arctan\left(\frac{DS_{\text{front}}^{\text{corr}} - DS_{\text{rear}}^{\text{corr}}}{d_{\text{Rear-Front}}}\right) \tag{2.1}$$

   where $d_r ear_f ront$ is the distance between rear and front DS measured with Geogebra. This angle represents the residual misalignment between the MIMU's anteroposterior axis and the true longitudinal axis of the foot.

5. Definition of the updated rotation matrix: Finally, a new rotation matrix (R_{calib}) is defined to realign all subsequent sensor data within the corrected coordinate system.

In summary, the new calibration represents an evolution of the method proposed by Rossanigo et al. (2023).
While the original approach assumed an ideal rigid geometry, the updated method explicitly compensates for mechanical deflection, sensor-specific offsets, and geometric asymmetries introduced by the new L-shaped support.
This refinement improves calibration accuracy and robustness, enabling the system to maintain precise alignment and reliable distance measurements even under variable mechanical and experimental conditions, a critical requirement for extending the system's applicability to pathological populations.

2.2.3 Definition of gait parameters: step length, stride width, and base of support area

The parameters under validation are defined as follows, consistent with the original work:

- Step Length: this is the linear distance between the footprints of two consecutive steps. Specifically, it is defined as the displacement along the direction of progression between a footprint centroid and the consecutive centroid of the opposite foot's footprint.

- Stride Width: This is the lateral distance between two consecutive footprints. It is determined as the perpendicular distance between a footprint's centroid and the direction of progression of the opposite foot.

- Base of Support Area (BoS): The BoS is defined as the area enclosed by the outer edges of the footprints during the double support phase. In the original

method, the footprints were approximated as rectangles, and the BoS area was calculated as the area of an irregular polygon formed by the vertices of the two footprints.

Figure 2.10 shows how the right and left stride width and step length are defined by this method, and Figure 2.11 shows the right and left base of support area.

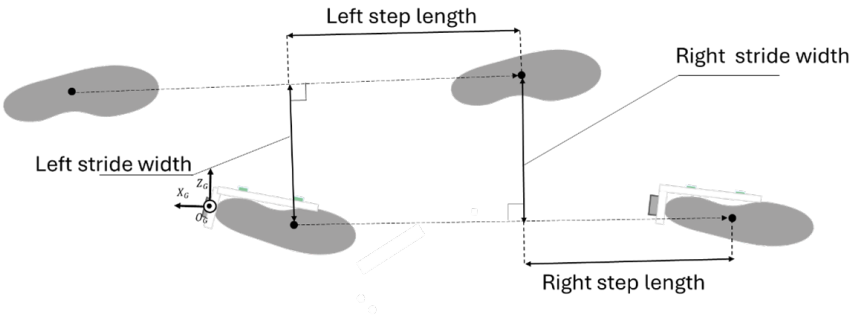

Figure 2.10: Definition of stride width and step length by [38]

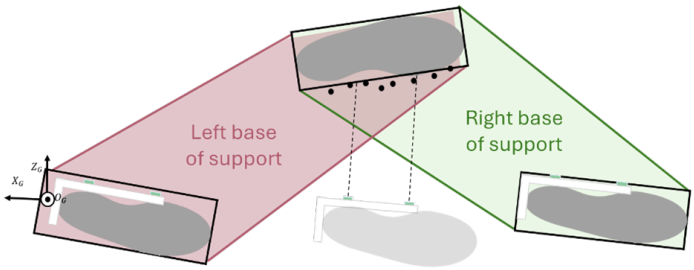

Figure 2.11: Definition of area of the base of support

2.2.4 Method by Wang et al. 2024 (M2)

As an additional benchmark, the deep learning model proposed by Wang et al. [41] was employed. This model was originally developed to estimate stride width in both healthy individuals and patients with neurodegenerative diseases, with the goal of reducing the need for complex instrumentation by relying on a minimal set of wearable inertial sensors (IMUs).
The architecture proposed by Wang et al. is based on a Recurrent Neural Network (RNN) LSTM (Long Short-Term Memory) designed to process time-series data from IMUs. A key element of the study was the introduction of a data-augmentation strategy to artificially increase training variability and improve model generalization across different subjects and pathological conditions. By combining raw sensor signals with statistical descriptors, the model integrates both low-level temporal

dynamics and higher-level summary features, enabling robust estimation of spatiotemporal gait parameters.
The setup consisted of three IMU, one positioned on the pelvis and the remaining two on the shanks as shown in figure 2.12.

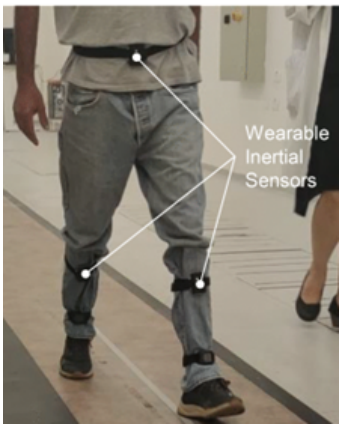

Figure 2.12: M2 setup

The model requires as input the segmented stance phases from the right foot (from heel strike to toe-off). Each stance phase is normalized to a fixed window length of 152 samples through zero-padding. The final input matrix has dimension $N \times 30$, where N is the total number of stance phases. The 30 features are organized as follows:

- 18 raw signals: 3D linear accelerations and 3D angular velocities for each IMU. In the original study, sensors were positioned on the shanks; in the present work, the sensors were mounted on the feet, but axes were arranged according to Wang et al.'s conventions (x ≈ mediolateral, y ≈ vertical, z ≈ anteroposterior). Although a discrepancy existed between sensor placement in the original study (shanks) and in the present setup (feet), the alignment of sensor axes was preserved to maintain consistency with the reference framework. Figure x illustrates the original axis configuration and the way in which the axes were later rearranged.

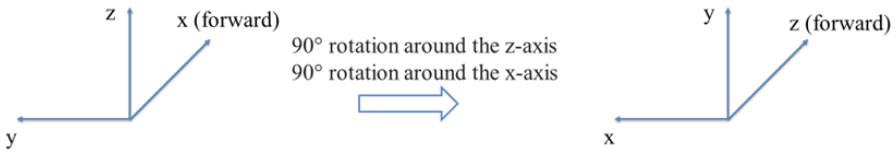

Figure 2.13: Rotation of the axes to provide the correct input signals for M2

- 12 features: mean value and L2-norm of each IMU channel, providing statistical descriptors to complement the raw time series.

Since they made available all the codes, the pretrained model was employed. To generate suitable inputs, right stance phases were first identified, segmented, and zero-padded. The resulting input matrices were then passed to the pretrained RNN, which produced estimates of stride width (in cm) for each stance phase.Figure x shows the workflow of M2.

Figure 2.14: Flowchart of M2 method

The model of Wang et al. was selected because it represents one of the first successful applications of deep learning to stride width estimation in both healthy and clinical populations. Also is one of the few studies that has made the codes available.
Its inclusion in this work provided a rigorous comparison for the proposed method, highlighting strengths and potential limitations with respect to an established algorithm trained on a large and diverse dataset.

2.2.5 Statistical analysis

Data Preprocessing and Normality Assessment
All data analyses were conducted using MATLAB (The MathWorks Inc., Natick, MA, USA). Measured parameters were analyzed across different methods (M1 vs M2), conditions (straight walking vs turning), sides (right vs left), and tests.
The assumption of normality for all resulting data vectors was initially assessed using the Shapiro-Wilk test (SWTEST). The null hypothesis (H_0) of a normal distribution was rejected for a p-value less than 0.05. An adaptive statistical approach was implemented based on the overall outcome of the normality check (represented by $\sum H$).
Comparison of Statistical Differences
To evaluate overall differences in the parameters across the various groups/conditions, the data underwent either parametric or non-parametric testing:

- Parametric Testing: if the assumption of normality was satisfied across all groups ($\sum H = 0$), the One-Way Analysis of Variance (ANOVA) was employed to compare the group means.

- Non-Parametric Testing: if the assumption of normality was violated in one or more groups $\sum H > 0$), the non-parametric Friedman test was performed as the appropriate alternative to the repeated measures ANOVA, comparing the median values across conditions.

Following a significant result in the main test ($p < 0.05$), post-hoc pairwise comparisons were conducted to identify which specific pairs of groups were significantly different. The Bonferroni correction was applied to adjust the p-values for multiple comparisons and maintain the Family-wise Error Rate (FWER) at the desired level.

Significance Level
Results were considered statistically significant if the p-value was less than 0.05. All continuous data are reported as mean ± standard deviation (SD) for normally distributed data, or as median and interquartile range (IQR) for non-normally distributed data.

2.3 Experimental instrumentation

To evaluate gait parameters and validate the estimation method under investigation (M1), multiple acquisition systems were employed. The INDIP system was used as the primary wearable device for capturing kinematic and pressure data during laboratory sessions. To provide a reference standard, a Vicon motion capture system was employed in the laboratory to obtain precise three-dimensional marker trajectories. In addition, the estimation method was compared against a reference machine learning model proposed by Wang et al. [41], which was implemented to benchmark performance against state-of-the-art approaches.
The combined use of these systems enabled the collection of complementary datasets: wearable sensor data in controlled and ecological conditions, gold-standard optical motion capture data for validation, and algorithmic estimations for benchmarking.

2.3.1 INDIP system

The INDIP system is a wearable sensing platform specifically designed for gait analysis in both laboratory and ecological settings. It integrates multiple inertial and pressure sensors to provide a comprehensive characterization of locomotor patterns. The configuration adopted in this study included:

- Four MIMU units (mod. LSMDSO and mod. LIS2MDL, STMicroelectronics, Switzerland; 3D accelerometer: range ±16 g; 3D gyroscope: range ±2000 dps; 3D magnetometer: range ±50 Gauss; sampling frequency: 100 Hz): two mounted on the feet, one positioned on the lower back at the level of the L5

vertebra, and one fixed to the left side of the head. Figure 2.15 show an IMU unit of the INDIP system.

Figure 2.15: MIMU of INDIP system

- One MIMU trigger unit used for synchronization of the acquisition.
- Two pressure insoles (PI): each equipped with an 18 cm flexible cable as Figure 2.16 shows. The left and right insoles were distinguished by different connector shapes to ensure correct placement. Orientation was guaranteed by positioning the black pads facing downward for the right insole and upward for the left.

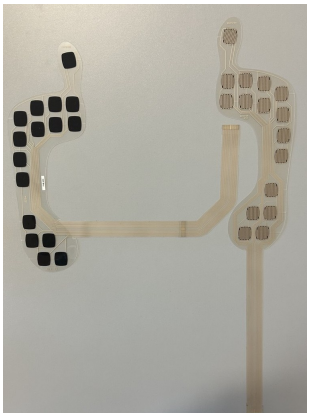

Figure 2.16: Force sensing resistor pressure insoles

- Two distance sensors (DS) (mod. VL6180X, STMicroelectronics, Switzerland; distance: range 0–200 mm; sampling frequency: 50 Hz) with corresponding connectors.
- Right-foot plastic support: designed to host one INDIP unit and the two DS, fixed to the medial side of the right shoe using screws and a Velcro strap

showed in Figure 2.17 and Figure 2.18. It consists of a 3D-printed rigid support with an "L" shape. The MIMU is positioned in the posterior section of the support, while the infrared ToF distance sensors are embedded on the medial arm, maintaining their orientation toward the contralateral foot.

Figure 2.17: Rigid support with two distance sensor and one IMU

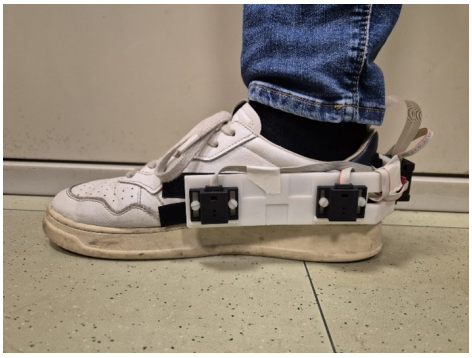

Figure 2.18: Complete setup of the right foot

- Clip for the left shoe: employed to secure the INDIP unit to the laces of the left shoe showed in Figure 2.19.

Figure 2.19: Setup of the left foot

This setup allowed the acquisition of spatiotemporal gait parameters through a combination of inertial measurements, pressure distribution data, and inter-sensor distance estimation. The portability and modularity of the system enabled its use both in controlled laboratory conditions and in out-of-lab scenarios, thus providing robust datasets for the validation of the proposed estimation method.

2.3.2 Vicon system

The Vicon motion capture system is one of the most used SP systems and is widely used in clinical and research settings for gait analysis. It was employed in this work thesis as the gold-standard reference for gait analysis in the laboratory environment. The system consisted of 12 infrared cameras positioned around the acquisition volume to ensure full coverage and to minimize marker occlusions. Cameras were calibrated prior to data collection to guarantee sub-millimeter spatial accuracy.
A total of 39 retro-reflective markers were placed on anatomical landmarks according to a standard full-body biomechanical model.

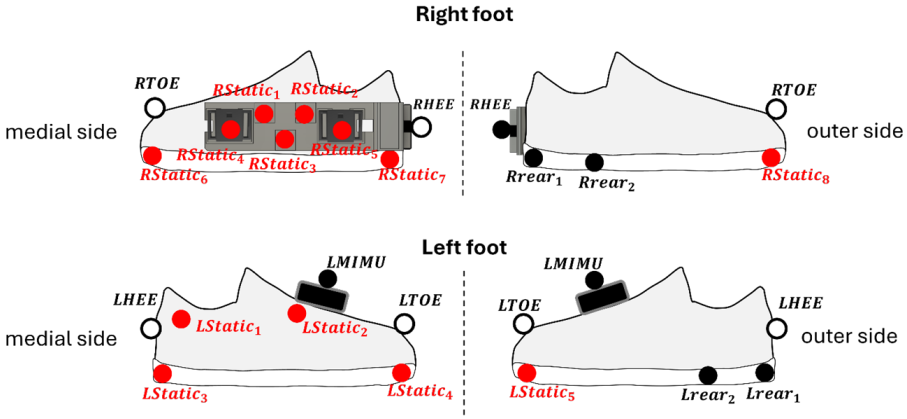

Figure 2.20: Right foot marker placement

Of these, 13 markers were temporary and used exclusively for static acquisitions in order to define joint centers and segment orientations; The figure 2.20 shows the temporary markers in red. The remaining 26 markers were retained for all dynamic tasks to capture lower- and upper-limb kinematics during gait. Among these, 16 markers corresponded to the lower-limb Plug-in Gait model showed in Figure 2.21.

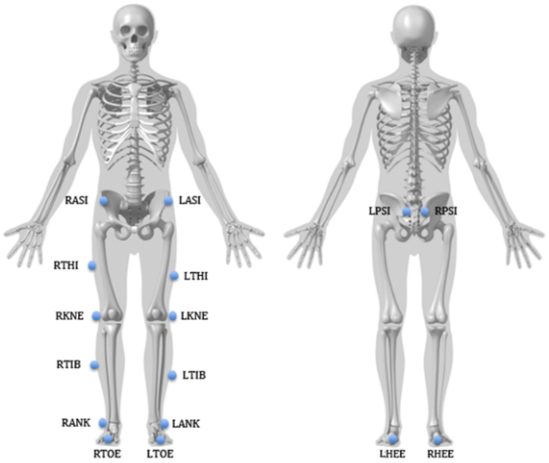

Figure 2.21: Plug-in gait model

The remaining 10 markers were positioned on feet, pelvis and head. These 26 markers represent a custom model that reproduces the segments of the human body as shown in Figure 2.22.

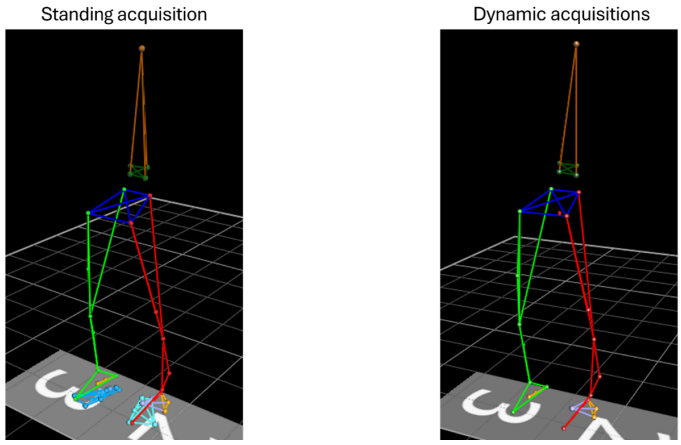

Figure 2.22: Reconstruction of marker trajectories by Nexus software

Data was collected at a sampling frequency of 100 Hz, and three-dimensional trajectories of the markers were reconstructed through the proprietary Vicon Nexus software. Example of gaps are showed in figure 2.23.

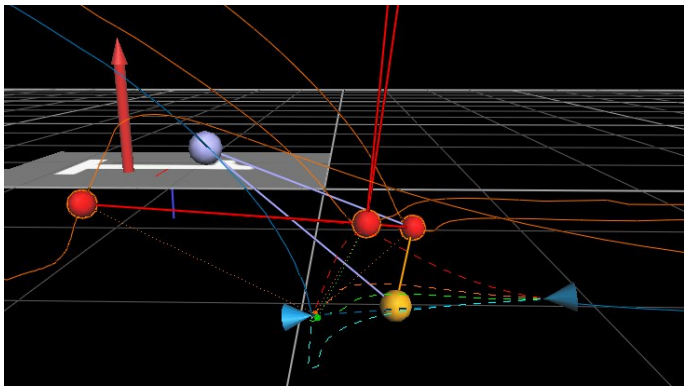

Figure 2.23: Example of a gap in marker trajectories reconstruction

Manual labeling was performed to ensure correct marker identification and to address potential occlusions during the trials. From the reconstructed trajectories, spatiotemporal gait parameters and joint kinematics could be derived.
Thanks to its high accuracy and reliability, the Vicon system served as the gold-standard reference for validating the measurements obtained from the wearable INDIP system, allowing a direct comparison between laboratory-grade optical motion capture and portable sensor-based acquisitions.

2.4 Experimental protocol

A total of 18 healthy subjects (9 females, 9 males), aged 20–62 years were enrolled in the study. Participants were recruited and assessed at Politecnico di Torino (PoliTO BIOMedLab). Inclusion criteria required the absence of musculoskeletal or neurological impairments potentially affecting gait, ensuring the ability to complete all experimental tasks.
The experimental protocol consists in a total of 8 tasks conducted in the laboratory and. Before the protocol begins, a static acquisition is performed for all INDIP sensors used in which an operator places all the devices on a flat surface and starts an acquisition of at least 60 seconds.
The tasks were designed to evaluate gait under various conditions and to provide a reference dataset for normative gait parameters.
All the tasks included in the experimental protocol are described in detail below.

1. Standing: participants were asked to stand upright without moving for 10 seconds. This task was intended to assess postural stability under static conditions.

2. Data personalization: this task can be performed in two versions, standing and seated designed to calibrate the acquisition system and evaluate balance and single-leg support.

    - Participants positioned the right foot on a plastic footprint and a box aligned with the dotted line beside the distance sensors. Acquisition started, and participants stood still for 10 seconds.

Figure 2.24: Position of the right foot during data personalization test

    - The box and footprint were removed, and participants remained standing

for at least 10 seconds.

- Participants lifted the left foot for at least 10 seconds (single right-leg support).
- Participants returned to double support for at least 5 seconds.
- Participants lifted the right foot for 10 seconds (single left-leg support).
- Participants returned to double support for at least 5 seconds.
- Finally, participants walked along a predefined "J"-shaped path.

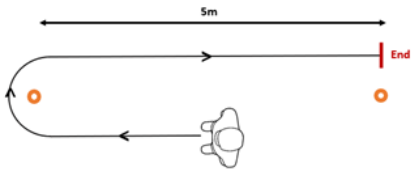

Figure 2.25: Data personalization test path

3. Straight walking: consists of 3 tasks performed at different speeds in which participants have to walk along a 5-meter linear path. Each task included two trials, with participants walking the path in both directions.

   - Comfortable: participants walked at their self-selected, comfortable walking speed.
   - Slow: participants walked at a deliberately slow pace, slower than their natural speed.
   - Fast: participants walked at a faster pace, faster than their self-selected comfortable speed.
     These tasks were designed to evaluate gait parameters under different walking speeds, providing a range of conditions for the validation of the estimation method.

Figure 2.26: Straight walking test path

4. The Timed Up and Go (TUG): this test is a widely used clinical assessment of a person's mobility. The participant is asked to sit in a chair, rise from a

seated position, walk straight to a cone placed 3 meters away, turn around the cone, and return to the chair, sitting down again at the end of the trial.

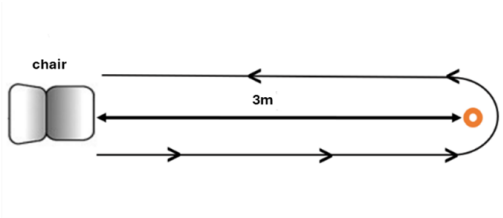

Figure 2.27: Time Up and Go test path

5. Two Minute Walk Test (2MWT): participants were asked to walk continuously for 2 minutes at a self-selected speed along a closed-loop path delimited by two cones placed 4 meters apart. At the end of the 2-minute period, participants returned to the starting point. This task is based on the standardized 2MWT, which is commonly used to assess functional exercise capacity and endurance in both healthy and clinical populations.

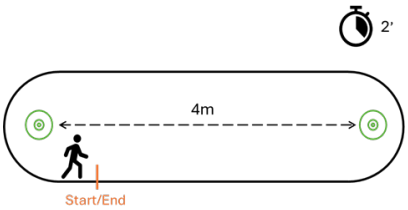

Figure 2.28: 2-Minute Walking test path

6. Hallway test: participants were instructed to stand at a designated starting point and walk along a 6 meters straight walkway. During the path, they were required to step up and down from a step positioned 4 meters away from the starting point. Upon reaching the end of the walkway, participants executed a sharp 180° turn and walked back along the same path again stepping up and down from the step, until reaching the endpoint. This task was designed to evaluate gait adaptability in response to vertical transitions and directional changes.

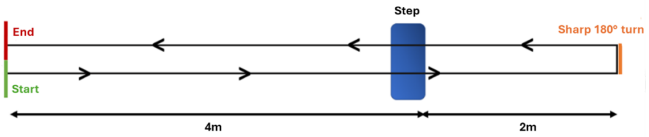

Figure 2.29: Hallway test path

7. 30-Second Chair Stand Test (30SCT): participants were seated on a chair with their arms crossed at the wrists. They were instructed to repeatedly stand up to a full upright position and sit back down, while always keeping both feet in contact with the ground. The test lasted 30 seconds, or a shorter duration if the participant was unable to continue. A lower number of repetitions is typically associated with reduced lower limb strength and a higher risk of falls, making this test a validated measure of functional mobility and muscle endurance.

Figure 2.30: 30-Second Chair Stand test path

8. Simulated Daily Activities (SDA): this task was designed to replicate a set of activities of daily living (ADL) within a controlled laboratory environment, in order to approximate real-world functional mobility demands. Given its complexity and the variety of interactions required, the task was structured into eight sequential steps:

   - Chair transfer: participants started sitting in a chair. They were instructed to stand up and walk to a cone positioned next to a table.
   - Table setting: participants were asked to set the table for dinner using the supplies placed on another table.
   - Chair carrying and rest: participants carried a chair to the last table, sat down, and took a short break with a drink (approximately 30–60 seconds).
   - Table clearing: participants cleared the table by returning all items to the other table.

- Diagonal walk with obstacles: participants walked diagonally across the laboratory, navigating around a series of cones arranged in the center of the floor.
- Straight walk with obstacle crossing: participants walked directly to a TV/laptop while stepping over an obstacle placed on the floor.
- Video watching / conversation: participants watched a 30–60 second video on the TV/laptop. In the absence of audiovisual equipment, a short conversation was conducted with the participant. If participants wished to sit before the end of the minute, a chair was provided by a researcher.
- Cone collection: participants collected all cones from the floor and returned to sit on the chair placed in the starting point. This complex task was intended to capture mobility, coordination, and multitasking abilities by integrating walking, object manipulation, obstacle negotiation, and short periods of rest into a single functional protocol.

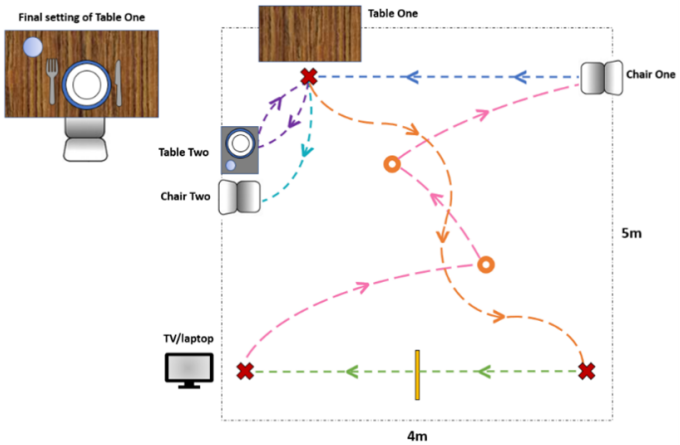

Figure 2.31: Simulated Daily Activities test path

Chapter 3

Results

This chapter presents the results of the validation analyses performed on healthy subjects.
Two main evaluations were performed:

- Section 3.1 reports the validation of Method 1 (M1) against the stereophotogrammetric gold standard for all estimated gait parameters—stride width, step length, and Base of Support (BoS) area.
- Section 3.2 compares the performance of M1 and Method 2 (M2) in estimating stride width, the only parameter computed by both approaches.

For all analyses, the following performance indicators were computed: mean value (MV) ± standard deviation (SD), mean error (ME) ± standard deviation , mean percentage error (MAE%) ± standard deviation (SD%), root mean square error (RMSE), and the Pearson correlation coefficient (r) with the stereophotogrammetric reference.

3.1 Validation of M1 against stereophotogrammetry

The first part of the analysis aimed to validate the performance of Method 1 (M1) in estimating stride width, step length, and base of support (BoS) area with respect to the stereophotogrammetric gold standard (SP).
This evaluation was carried out on all experimental conditions under different walking speeds and conditions, such as straight walking and turning, to assess both the precision and robustness of the proposed method. Figure 3.1, 3.2 and 3.3 show the comparison between M1 and SP of each BoS parameters estimation during straight walking.

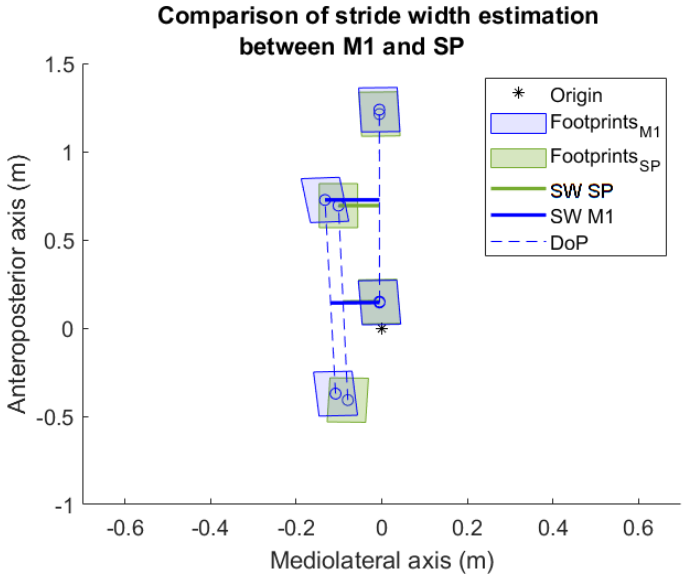

Figure 3.1: Stride width estimation with M1 method during straight walking

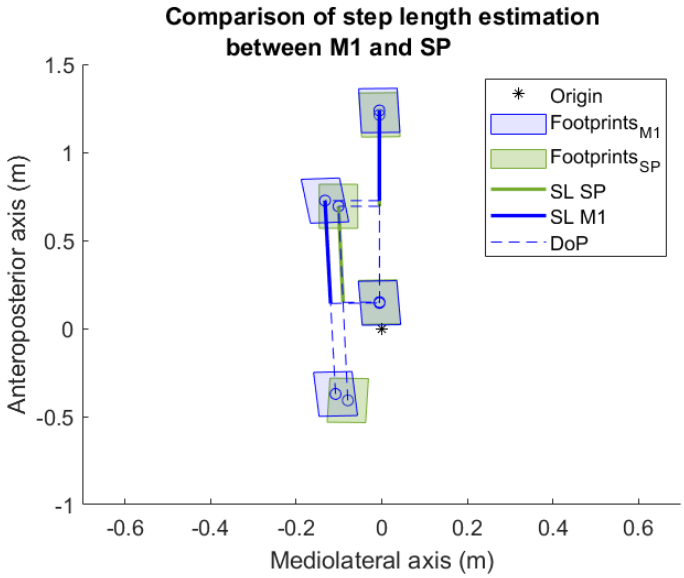

Figure 3.2: Step length estimation with M1 method during straight walking

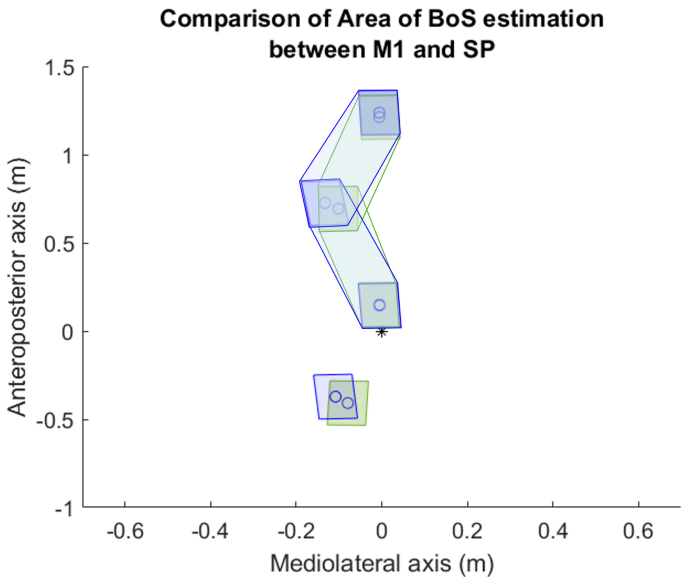

Figure 3.3: Area of BoS estimation with M1 method during straight walking

Figure 3.4 shows the same comparison of BoS parameters estimation in the turning condition.

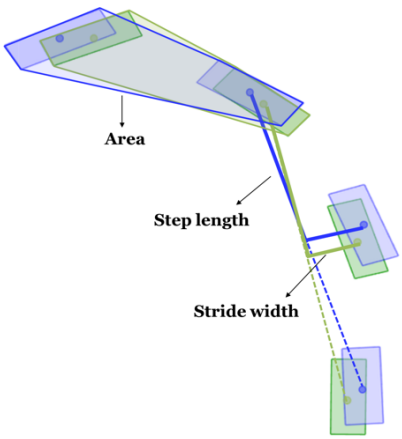

Figure 3.4: Estimation of all BoS parameters turning

3.1.1 Comparison between straight walking at three different speeds

The first analysis investigated the effect of walking speed on the estimation accuracy of the three gait parameters.
Participants performed straight walking trials at three self-selected speeds: slow, comfortable, and fast.
For each condition, the mean and standard deviation of the estimated parameters were computed, along with error metrics and correlation values with the reference system.

Stride width
Stride width values for all conditions and sides are reported in Table 3.1.
For the comfortable, slow, and fast walking tests, the MV, ME, RMSE, MAE%, and Pearson's correlation coefficients showed consistent trends across sides and speeds. ME error is between 0.024 m and 0.038 m and the Pearson coefficient ranges from 0.82 to 0.95.

Tests names	**Side**	**Metrics**	**Straight walking**	**All (Right and Left)**
SW conf	Right	MV±SD (m)	0.162 ± 0.034	0.164 ± 0.035
		ME±SD (m)	0.036 ± 0.020	$0.037 \pm 0.020^{**}$
		RMSE (m)	0.042	0.042
		MAE±SD (%)	31.5 ± 16.6	$30.8 \pm 16.4^{**}$
		r_{xy}	0.83	0.82
	Left	MV±SD (m)	0.173 ± 0.038	0.164 ± 0.035
		ME±SD (m)	0.038 ± 0.022	$0.037 \pm 0.020^{**}$
		RMSE (m)	0.043	0.042
		MAE±SD (%)	28.5 ± 15.9	$30.8 \pm 16.4^{**}$
		r_{xy}	0.82	0.82
SW slow	Right	MV±SD (m)	0.154 ± 0.042	0.155 ± 0.041
		ME±SD (m)	$0.030 \pm 0.015^{*}$	$0.029 \pm 0.015^{**}$
		RMSE (m)	0.034	0.032
		MAE±SD (%)	$26.8 \pm 15.7^{*}$	$25.1 \pm 15.1^{**}$
		r_{xy}	0.93	0.93
	Left	MV±SD (m)	0.154 ± 0.041	0.155 ± 0.041
		ME±SD (m)	$0.024 \pm 0.014^{*}$	$0.029 \pm 0.015^{**}$
		RMSE (m)	0.027	0.032
		MAE±SD (%)	$20.3 \pm 12.5^{*}$	$25.1 \pm 15.1^{**}$
		r_{xy}	0.95	0.93
SW fast	Right	MV±SD (m)	0.170 ± 0.054	0.169 ± 0.053
		ME±SD (m)	0.034 ± 0.021	0.034 ± 0.024
		RMSE (m)	0.040	0.042
		MAE±SD (%)	28 ± 18.4	28.8 ± 19.1
		r_{xy}	0.92	0.89
	Left	MV±SD (m)	0.168 ± 0.050	0.169 ± 0.053
		ME±SD (m)	0.036 ± 0.030	0.034 ± 0.024
		RMSE (m)	0.046	0.042
		MAE±SD (%)	30.9 ± 21.1	28.8 ± 19.1
		r_{xy}	0.82	0.89

Table 3.1: Stride width metrics for straight walking and combined (right and left) conditions for comfortable, slow and fast speed.

According to the Shapiro-Wilk test, stride width errors were normally distributed for comfortable and fast tests and non-normally distributed for slow tests. In comfortable and fast walking conditions, no statistically significant differences were found between the right and left side parameters. In contrast, a significant side difference emerged in the slow walking test ($p < 0.05$). Additionally, when comparing walking speeds in the combined-side analysis (All), a significant difference was observed between the comfortable-speed test (Test 4) and the slow-speed test (Test 5) ($p < 0.05$).

Step length

Step length results for all walking conditions are summarized in Table 3.2.
The results show that the ME error is between 0.037 m and 0.111 m and the Pearson coefficient ranges from 0.73 to 0.92.

Tests names	**Side**	**Metrics**	**Straight walking**	**All (Right and Left)**
SW conf	Right	MV±SD (m)	0.577 ± 0.082	0.607 ± 0.098
		ME±SD (m)	$0.064 \pm 0.057^{*}$	$0.025 \pm 0.092^{**}$
		RMSE (m)	0.085	0.095
		MAE±SD (%)	$11.1 \pm 7^{*}$	$12.8 \pm 7.9^{**}$
		r_{xy}	0.73	0.48
	Left	MV±SD (m)	0.711 ± 0.079	0.607 ± 0.098
		ME±SD (m)	$0.111 \pm 0.053^{*}$	$0.025 \pm 0.092^{**}$
		RMSE (m)	0.121	0.095
		MAE±SD (%)	$18.6 \pm 8.5^{*}$	$12.8 \pm 17.9^{**}$
		r_{xy}	0.74	0.48
SW slow	Right	MV±SD (m)	0.478 ± 0.084	0.499 ± 0.089
		ME±SD (m)	$0.037 \pm 0.043^{*}$	$0.010 \pm 0.061^{**}$
		RMSE (m)	0.057	0.061
		MAE±SD (%)	$8.2 \pm 7^{*}$	$9.8 \pm 7.4^{**}$
		r_{xy}	0.86	0.75
	Left	MV±SD (m)	0.551 ± 0.078	0.499 ± 0.089
		ME±SD (m)	$0.060 \pm 0.036^{*}$	$0.010 \pm 0.061^{**}$
		RMSE (m)	0.070	0.061
		MAE±SD (%)	$13.6 \pm 7.5^{*}$	$9.8 \pm 7.4^{**}$
		r_{xy}	0.90	0.75
SW fast	Right	MV±SD (m)	0.611 ± 0.16	0.671 ± 0.185
		ME±SD (m)	$0.087 \pm 0.069*$	0.031 ± 0.117
		RMSE (m)	0.11	0.120
		MAE±SD (%)	$14.5 \pm 8^{*}$	15.2 ± 8.4
		r_{xy}	0.92	0.78
	Left	MV±SD (m)	0.825 ± 0.141	0.671 ± 0.185
		ME±SD (m)	$0.111 \pm 0.089^{*}$	0.031 ± 0.117
		RMSE (m)	0.141	0.120
		MAE±SD (%)	$16.8 \pm 9.3^{*}$	15.2 ± 8.4
		r_{xy}	0.80	0.78

Table 3.2: Step length metrics for straight walking and combined (right and left) conditions for comfortable, slow and fast speed.

According to the Shapiro-Wilk test, step length errors were normally distributed for comfortable and fast tests and non-normally distributed for slow tests. Across all three tests, comfortable, slow, and fast, a statistically significant difference between the right and left side parameter was found ($p < 0.05$). These side-specific differences were consistent across all parameters reported in the table.
When analyzing the combined sides (all), a significant difference between Test 4 (comfortable) and Test 5 (slow) was detected ($p < 0.05$). No significant differences were found between Test 4 and Test 6 or between Test 5 and Test 6.

AreaBoS

AreaBoS results for each walking condition are presented in Table 3.3.
Results show that the ME is between 0.004 m^2 e 0.039 m^2 and the Pearson coefficient ranges from 0.65 from 0.91.

Tests names	**Side**	**Metrics**	**Straight walking**	**All (Right and Left)**
SW conf	Right	MV±SD (m^2)	0.125 ± 0.026	0.145 ± 0.036
		ME±SD (m^2)	$0.008 \pm 0.016^{*}$	0.014 ± 0.029
		RMSE (m^2)	0.018	0.032
		MAE±SD (%)	$11 \pm 7.5^{*}$	$20.4 \pm 13.2^{**}$
		r_{xy}	0.8	0.61
	Left	MV±SD (m^2)	0.167 ± 0.033	0.145 ± 0.036
		ME±SD (m^2)	$0.039 \pm 0.016^{*}$	0.014 ± 0.029
		RMSE (m^2)	0.042	0.032
		MAE±SD (%)	$30.5 \pm 10.2^{*}$	20.4 ± 113.2
		r_{xy}	0.91	0.61
SW slow	Right	MV±SD (m^2)	0.115 ± 0.022	0.128 ± 0.028
		ME±SD (m^2)	$0.004 \pm 0.011^{*}$	$0.012 \pm 0.020^{**}$
		RMSE (m^2)	0.011	0.023
		MAE±SD (%)	$8.4 \pm 5^{*}$	17 ± 11.8
		r_{xy}	0.91	0.72
	Left	MV±SD (m^2)	0.141 ± 0.028	0.128 ± 0.028
		ME±SD (m^2)	$0.028 \pm 0.011^{*}$	0.012 ± 0.020
		RMSE (m^2)	0.030	0.023
		MAE±SD (%)	$25.7 \pm 10.3^{*}$	17 ± 11.8
		r_{xy}	0.91	0.72
SW fast	Right	MV±SD (m^2)	0.132 ± 0.029	0.156 ± 0.041
		ME±SD (m^2)	$0.012 \pm 0.019*$	0.014 ± 0.033
		RMSE (m^2)	0.023	0.036
		MAE±SD (%)	$11.7 \pm 8.9^{*}$	20.7 ± 14.9
		r_{xy}	0.80	0.65
	Left	MV±SD (m)	0.180 ± 0.037	0.156 ± 0.041
		ME±SD (m)	$0.039 \pm 0.022^{*}$	0.014 ± 0.033
		RMSE (m)	0.045	0.036
		MAE±SD (%)	$29.6 \pm 14.5^{*}$	20.7 ± 14.9
		r_{xy}	0.80	0.65

Table 3.3: Area of BoS metrics for straight walking and combined (right and left) conditions for comfortable, slow and fast speed.

According to the Shapiro-Wilk test, area of the base of support errors were normally distributed for comfortable and fast tests and non-normally distributed for slow tests.
Significant differences between the right and left limbs were found in all three tests—comfortable, slow, and fast walking ($p < 0.05$). These differences were consistent across all the metrics reported. No statistically significant differences were identified between tests in the combined-limb analysis.

3.1.2 Comparison between straight and curvilinear paths of all tests

The second analysis focused on comparing the estimation accuracy of M1 during straight and curvilinear walking tasks.
This test aimed to evaluate the method's robustness when the walking trajectory deviates from linear motion, and the relative orientation of the feet changes continuously.
Stride width values for straight and turning trials, including the combined condition, are reported in Table 3.4.

	Metrics	**Straight walking**	**Turning**	**All (Straight+Turn)**	**All Straight (Right+Left)**	**All Turn (Right and Left)**
Right	MV±SD (m)	0.163±0.05	0.164±0.079	0.163±0.067	0.182±0.070	0.226±0.115
	ME±SD (m)	0.033±0.027*	0.010±0.044*	0.010±0.043*	0.030±0.035	0.021±0.052
	RMSE (m)	0.042	0.046	0.044	0.045	0.056
	MAE±SD (%)	31.6±20.2*	26±18.7*	28.7±19.6*	28.8±20.3	28.1±20.5
	r_{xy}	0.86	0.86	0.83	0.88	0.89
Left	MV±SD (m)	0.206±0.083	0.278±0.114	0.252±0.110	–	–
	ME±SD (m)	0.028±0.043*	0.048±0.042*	0.040±0.043*	–	–
	RMSE (m)	0.050	0.063	0.059	–	–
	MAE±SD (%)	25.1±19.7*	29.6±21.9*	28.2±21.2*	–	–
	r_{xy}	0.86	0.93	0.92	–	–

Table 3.4: Stride width metrics for right and left tests during straight walking, turning, and combined conditions.

Overall, mean values and associated error metrics showed increased variability during turning, particularly for the left component, reflecting the additional medio-lateral adjustments required in curvilinear locomotion. The boxplots shown in figure 3.5 represent errors in straight and curved walking. It can be seen that the median errors are comparable in the two walking conditions (0.03m), but there is more variability in the error during turning, due to its non-standard pattern.

Figure 3.5 shows the stride width errors in both walking condition.

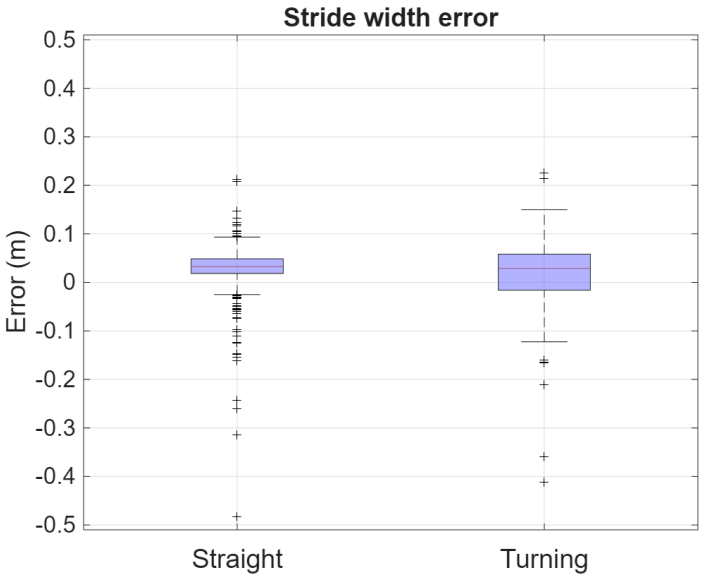

Figure 3.5: Stride width errors of M1 method during straight walking and turning in all tests

The correlation with stereophotogrammetry of both straight walking and turning was found to be very high ($\rho = 0.90$), as shown in the figure 3.6.

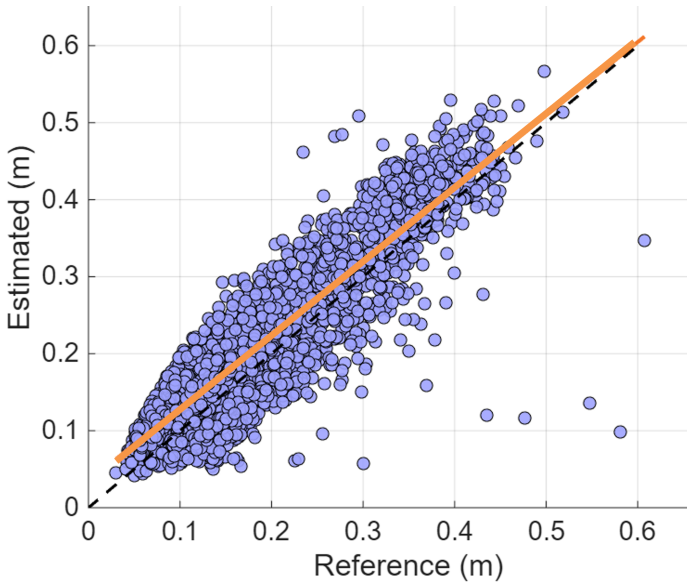

Figure 3.6: Stride width correlation

Statistical analyses revealed significant differences between the right and left components in both the straight and turning conditions ($p < 0.05$). When considering straight and turning together (combined condition), significant right–left differences were also present.
However, when the two components were averaged (all), no statistically significant differences were detected between straight and turning walking. This suggests that although each side of the parameter behaves differently between straight and turning trajectories, the combined measure remains stable across conditions.

Step length results are reported in Table 3.5 for straight, turning, and combined paths.

	Metrics	**Straight walking**	**Turning**	**All (Straight+Turn)**	**All Straight (Right+Left)**	**All Turn (Right and Left)**
Right	MV±SD (m)	0.538±0.088	0.492±0.104	0.510±0.010	0.597±0.118	0.538±0.132
	ME±SD (m)	0.060±0.051*	0.043±0.054*	0.050±0.053*	0.013±0.103*	0.020±0.094*
	RMSE (m)	0.079	0.069	0.073	0.104	0.096
	MAE±SD (%)	10.9±7.1*	10±7.5*	10.3±7.4*	15.1±10.3*	15.2±12.8*
	r_{xy}	0.84	0.87	0.86	0.65	0.71
Left	MV±SD (m)	0.678±0.105	0.589±0.142	0.620±0.136	–	–
	ME±SD (m)	0.112±0.064*	0.090±0.078*	0.098±0.074*	–	–
	RMSE (m)	0.129	0.119	0.123	–	–
	MAE±SD (%)	25.1±19.7*	29.6±21.9*	28.2±21.2*	–	–
	r_{xy}	0.80	0.84	0.85	–	–

Table 3.5: Step length metrics for right and left tests during straight walking, turning, and combined conditions in all tests.

As expected, turning trials showed a reduction in step length for both sides compared to straight walking, consistent with typical behavior during curved-path locomotion. Statistically significant differences between the right and left components were observed in both straight and turning walking ($p < 0.05$). In addition, a significant difference emerged between straight and turning when the combined measure right and left was analyzed, indicating that turning consistently modifies step-length patterns at the global level. Furthermore, when straight and turning trials were analyzed together, significant right–left differences persisted, confirming that the asymmetry between the two sides of the step-length parameter is robust across path geometries. Figure 3.7 shows the step length errors in both walking condition

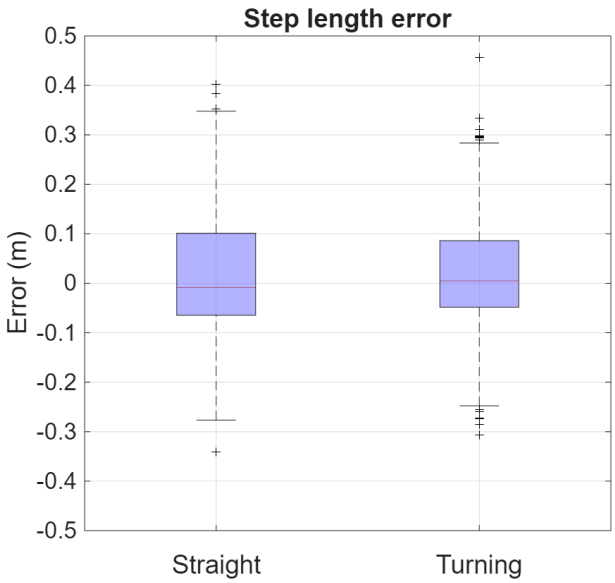

Figure 3.7: Step length errors of M1 method during straight walking and turning

The correlation with stereophotogrammetry of both straight walking and turning was found to be moderate ($\rho = 0.68$), as shown in the figure 3.8.

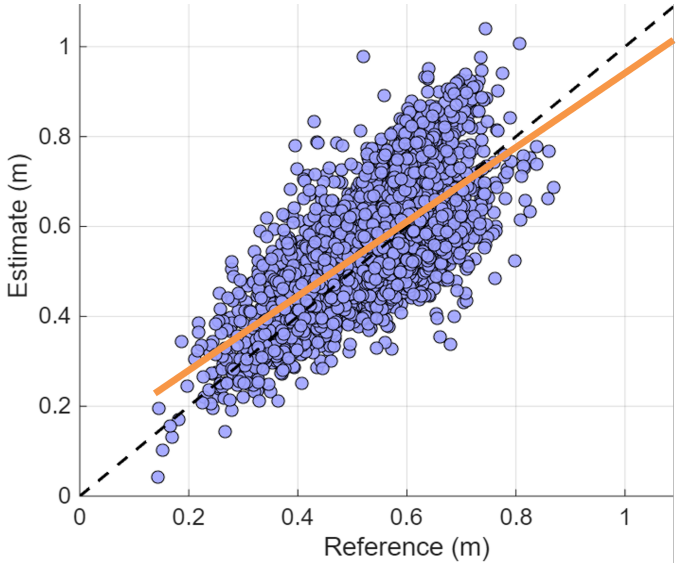

Figure 3.8: Step length correlation

AreaBoS results are summarized in Table 3.6.

	Metrics	Straight walking	Turning	All (Straight+Turn)	All Straight (Right+Left)	All Turn (Right and Left)
Right	MV±SD (m^2)	0.120±0.025	0.123±0.023	0.122±0.024	0.143±0.039	0.149±0.041
	ME±SD (m^2)	0.010±0.018*	0.014±0.018*	0.012±0.018*	0.012±0.030*	0.007±0.029*
	RMSE (m^2)	0.021	0.023	0.022	0.032	0.03
	MAE±SD (%)	10.8±8.2*	11.7±8.9*	11.4±8.6*	19.8±13.9*	16.4±11.7*
	r_{xy}	0.81	0.74	0.77	0.65	0.72
Left	MV±SD (m^2)	0.166±0.037	0.175±0.039	0.171±0.039	–	–
	ME±SD (m^2)	0.035±0.021*	0.029±0.019*	0.032±0.020*	–	–
	RMSE (m^2)	0.041	0.035	0.038	–	–
	MAE±SD (%)	28.9±12.4*	21.3±12.2*	24.3±12.8*	–	–
	r_{xy}	0.83	0.87	0.85	–	–

Table 3.6: Area of BoS metrics for right and left tests during straight walking, turning, and combined conditions in all tests.

Similar to step length, AreaBoS displayed increased variability during turning, particularly for the left component, reflecting the larger adjustments in foot placement required when changing direction.
The statistical outcomes mirrored those of step length. Significant differences between right and left components were found in both straight and turning walking ($p < 0.05$). Additionally, significant differences between straight and turning walking were detected in the combined (all) analysis. When straight and turning trials were considered together, right–left differences remained statistically significant, confirming that the asymmetrical behaviour of the parameter persists across path conditions. Figure 3.8 shows the area of BoS errors in both walking condition

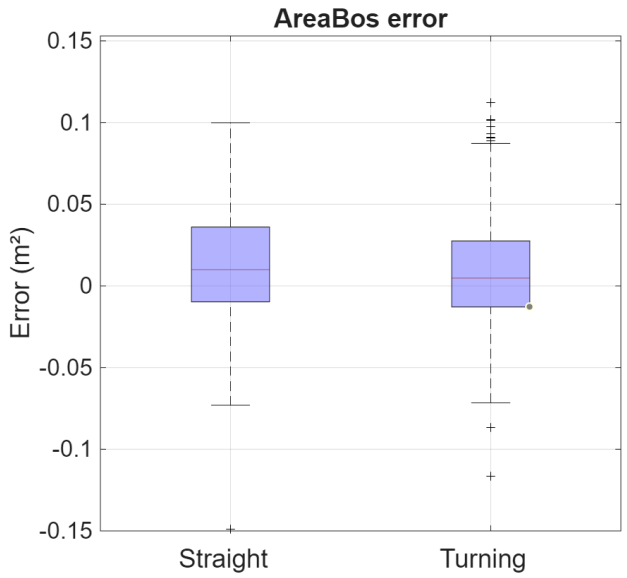

Figure 3.9: Area BoS errors of M1 method during straight walking and turning

The correlation with stereophotogrammetry of both straight walking and turning was found to be moderate ($\rho = 0.69$), as shown in the figure 3.9.

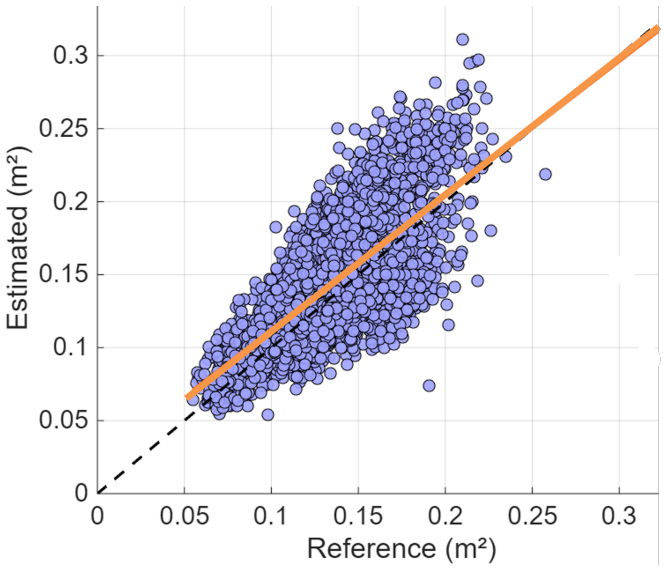

Figure 3.10: Area of BoS correlation

3.2 Comparison between M1 and M2

The second part of the analysis compared M1 and M2 in estimating stride width, which is the only gait parameter computed by both methods. While M1 relies on a deterministic geometrical approach based on sensor fusion and spatial reconstruction, M2 employs a machine learning model trained to predict stride width directly from MIMU and distance sensor data. Both methods were validated against the stereophotogrammetric reference under the same experimental conditions.
For each trial, mean and percentage errors, RMSE, and correlation coefficients were calculated and compared.

Stride width values for straight and turning trials, including the combined condition, are reported in Table 3.7.

	Metrics	**Straight walking**	**Turning**	**All (Straight+Turn)**	**All Straight (Right+Left)**	**All Turn (Right and Left)**
Right	MV±SD (m)	0.155±0.081	0.165±0.095	0.161±0.089	0.179±0.088	0.194±0.098
	ME±SD (m)	0.005±0.083*	0.023±0.108*	0.011±0.100*	0.005±0.092	0.036±0.011
	RMSE (m)	0.083	0.112	0.100	0.092	0.119
	MAE±SD (%)	41.1±27.4*	43.9±26.2*	42.7±26.8*	40.2±26.7	40.5±24.4
	r_{xy}	0.42	0.31	0.35	0.41	0.34
Left	MV±SD (m)	0.214±0.087	0.220±0.094	0.217±0.091	–	–
	ME±SD (m)	0.004±0.103*	0.047±0.118*	0.031±0.116*	–	–
	RMSE (m)	0.103	0.127	0.120	–	–
	MAE±SD (%)	39±25.7*	37.6±22.3*	38±23.4*	–	–
	r_{xy}	0.22	0.24	0.23	–	–

Table 3.7: Stride width metrics for right and left tests during straight walking, turning, and combined conditions in all tests.

Across all conditions, the mean error (ME) remained relatively small for both the right and left components, although with considerable variability, especially during turning. The MAE% values were high in all datasets, reflecting substantial relative error despite the limited absolute magnitude of the ME.
The Pearson correlation coefficients showed consistently weak associations between M2 and the reference system. For the right component, correlations remained low across straight, turning, and combined conditions, and similarly low values were observed in the aggregated "all straight" and "all turn" analyses. The left component exhibited even lower correlations, with values indicating very limited linear agreement with the reference measurements across all path types. Overall, stride-width estimates produced by Method M2 were characterised by small mean

errors but high relative errors and weak correlations with the reference system in both straight and curvilinear walking.
A statistical comparison was conducted between M1 and M2 by analysing stride width with right and left components aggregated. According to the Shapiro-Wilk test, stride width errors were non-normally distributed, so a Friedmann test was computed. This analysis provides further evidence of the difference in performance between the two methods. No significant difference was found between straight and turning walking using M1. Instead the same comparison for M2 show a significant difference between straight and turning ($p < 0.5$). A highly significant difference ($p < 0.5$) emerged when comparing M1 and M2 in straight walking and turning, indicating that M2 diverges substantially from M1 under both gait conditions. The box plots shown in figure x show that the error variability for method M1 is much lower than for method M2 in both walking conditions.

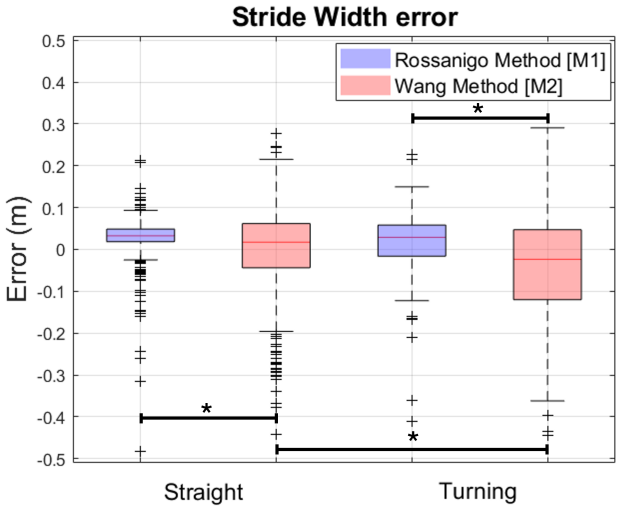

Figure 3.11: Comparison of stride width errors between M1 and M2 during straight walking and turning in all tests

The correlation with stereophotogrammetry of both straight walking and turning was found to be low ($\rho \approx 0.34$)

Chapter 4

Discussion

4.1 M1 performances

The section aimed to evaluate the performance of M1 in estimating key spatial gait parameters, stride width, step length, and the Area of the Base of Support (AreaBoS), under three straight-walking conditions: comfortable, slow, and fast speeds. The results obtained were analyzed in terms of accuracy (mean error and RMSE), variability, limb-specific differences, and consistency across walking speeds. By comparing right and left limb measurements, as well as aggregated (all) values across tests, it was possible to identify both systematic asymmetries and speed-related modulations.
Correlation analyses provided additional insight into the agreement between M1 and the reference system, highlighting conditions in which the measurement reliability improved or deteriorated. These findings collectively contribute to a more nuanced understanding of M1's performance across different locomotor contexts and help identify where the system is most stable.

4.1.1 Comparison between straight walking at three different speeds

Below, the behavior of each parameter is discussed with respect to the three walking speeds, including considerations related to correlation coefficients (r), which reflect the strength of agreement between M1 and the reference measurements.

Stride width showed relatively stable behavior across comfortable and slow walking, where both accuracy measures and correlations indicated reliable performance of M1. In these conditions, the correlations were consistently high ($r \approx 0.82^{\sim}0.95$), demonstrating a strong linear relationship between M1 and the reference system.

This suggests that when gait is performed at a natural or slow pace—characterized by smoother medio-lateral control and more predictable foot placement—M1 can capture stride width with good consistency.
In contrast, fast walking presents a different pattern. Not only were right–left side differences statistically significant, but the dynamics of the movement reduced the overall predictability of foot positioning. Despite this increased variability, correlation remained high ($r \approx 0.82\check{}0.92$), which indicates that the system remained consistent even if the side asymmetry increased. In other words, though fast walking introduces variability in absolute values, the relationship between the two measurement systems remains strong. This suggests that M1 responds reliably to changes in stride width even under challenging, low-speed conditions.
Overall, correlation trends confirm that stride width is the parameter with the most stable linear agreement across speeds.

Step length exhibited more pronounced variability and persistent asymmetry across all speeds, as highlighted by the significant side differences. The correlations reflected this complexity. In the comfortable and fast walking conditions, correlations ranged from moderate to high depending on the side ($r \approx 0.73 - 0.92$), indicating reasonable but less uniform agreement than observed for stride width. These fluctuations likely reflect the difficulty of capturing step length consistently when gait speed increases and dynamic oscillations of the lower limbs become more pronounced.
The slow walking condition showed moderately high correlations ($r \approx 0.75 - 0.90$), which, again, suggests good agreement but also some sensitivity to the reduced forward momentum characteristic of slow gait. Overall, although step length correlations are satisfactory, they show greater variability across speeds and between side. This indicates that step length is a more challenging parameter for M1 to estimate symmetrically and consistently, likely because of the increased dependence on accurate gait-event detection.

AreaBoS presented the highest degree of side asymmetry and also the most pronounced variability across the three conditions. These fluctuations were clearly reflected in the correlation coefficients, which were consistently lower than those of stride width and step length. Comfortable and fast walking yielded moderate correlations ($r \approx 0.65 - 0.80$), suggesting a weaker linear relationship between the two measurement systems. This result is not surprising, since AreaBoS combines both medio-lateral and anterior–posterior components, amplifying errors or inconsistencies in either stride width or step length.

Interestingly, slow walking showed higher correlations ($r \approx 0.72 - 0.91$), which may indicate that despite its variability, the reduced walking speed stabilizes the temporal sequencing of foot placement, improving the internal consistency of AreaBoS estimation. Nevertheless, the overall lower correlation values across tests reflect the complexity of the parameter: as a composite measure, AreaBoS inherently accumulates uncertainties from both directional components, making it more susceptible to speed- and side-dependent fluctuations.
It is important to consider that, in the present study, only the right foot was instrumented with the M1 system, while the parameters of the left foot were derived indirectly. This methodological choice may have contributed to the asymmetries observed across several gait parameters—particularly step length and the Area of the Base of Support. Therefore, the asymmetries observed in the results may not necessarily reflect true biomechanical differences in gait, but rather differences in measurement fidelity between the directly instrumented foot and the non-instrumented one.

4.1.2 Comparison between straight and curvilinear walking

The comparison between straight and curvilinear paths across all tests provides important insights into how M1 behaves under different locomotor geometries. Turning walking introduces additional biomechanical challenges, including medio-lateral adjustments, asymmetrical foot placement, and altered step timing, that naturally increase gait variability. These modifications have a direct impact on the estimation of spatial gait parameters, and consequently on the consistency between the right and left components of each measure.
The presence of statistically significant differences between right and left parameter components in both straight and turning walking suggests that M1's estimation is sensitive to asymmetrical modulation of gait, particularly when the system must reconstruct the non-instrumented side. Correlation trends further highlight how path geometry influences the agreement between M1 and the reference system, with turning generally producing equal or slightly reduced correspondence due to increased kinematic complexity.
The following sections discuss these results in detail for each parameter.

Stride width behaved differently between its right and left components in both straight and turning walking, as reflected by the statistically significant right–left differences. These findings indicate that turning amplifies the asymmetry inherent to the parameter's estimation. Because stride width depends on medio-lateral foot placement, turning requires the outer side to widen its trajectory while the inner side reduces it. This produces an intrinsic asymmetry in the spatial configuration of

the base of support, which is further accentuated by the unilateral instrumentation of M1.
Correlation values remained generally high across both path types, indicating that despite these asymmetries, M1 preserved good consistency relative to the reference system. This suggests that the system can track medio-lateral adjustments reliably even when path geometry becomes more complex.
Interestingly, when both components were combined, no significant differences were observed between straight and turning. This indicates that the global stride-width measure averages out the inherent asymmetries generated during turning, leading to a stable overall behaviour of the parameter. Therefore, while stride width is sensitive to local (side-specific) variations, it remains robust when interpreted at a global level.

Step length exhibited significant right–left differences in both straight and turning walking, confirming that asymmetry is a persistent characteristic of this parameter within M1. Turning typically reduces step length on the inner trajectory and may increase it on the outer one; thus, the significant differences between straight and turning in the combined analysis reflect well-established biomechanical adaptations associated with curvilinear gait.
From a methodological standpoint, M1 directly senses the right-side step events while reconstructing the left-side step timings. Turning increases temporal variability, particularly in the inner step, making the reconstruction process more challenging and amplifying side differences. This helps explain the systematic asymmetry observed even in straight walking, and the additional modifications seen during turning.
Correlation coefficients were moderate to high, but slightly lower in turning conditions, consistent with the increased step-to-step variability. This reduction likely reflects the greater difficulty in detecting consistent gait events in curvilinear trajectories and the compounded effect of reconstructing the non-instrumented side.
Overall, step length emerges as the parameter most affected by turning, both biomechanically and methodologically.

AreaBoS displayed a pattern very similar to step length, with significant right–left differences in both straight and turning walking and significant differences between straight and turning at the combined level. This is expected, as AreaBoS integrates both stride width and step length into a composite measure, and thus accumulates the asymmetries and variabilities present in the two underlying components.
Turning inherently alters the geometry of the base of support. The inner side typically shortens its step and narrows its placement, while the outer side widens and lengthens its trajectory. This asymmetrical modulation directly impacts the area

enclosed between successive foot placements, explaining the observed differences in both sides of the parameter.
Correlations for AreaBoS were moderate and tended to decrease during turning. This reduction is consistent with the compound nature of the parameter: any imprecision in stride width or step length—especially on the non-instrumented side—propagates and is magnified when computing the area.
Given these considerations, AreaBoS should be interpreted with caution, particularly in curvilinear contexts where the combination of biomechanical asymmetry and unilateral instrumentation introduces additional complexity.

4.1.3 Comparison between M1 and M2 for stride-width estimation

The comparison between M1 and M2 reveals substantial differences in the fidelity with which the two methods estimate stride width across straight and curvilinear walking tasks. Although both methods produced mean errors of similar magnitude, their performance diverged sharply when considering MAE% and the correlation with the reference system.

Across all walking conditions, M1 consistently demonstrated superior agreement with reference measurements. In straight walking, M1 achieved an RMSE of 4.7 cm, which, although higher than the 3.5 cm RMSE reported by Wang et al. for their original model, remains within an acceptable range given differences in instrumentation and experimental design. During turning, where Wang et al. did not provide validation data, M1 maintained reasonable performance with an RMSE of 5.6 cm. In both locomotor conditions, M1 exhibited moderate MAE% and Pearson correlation coefficients ranging from moderate to high, indicating that stride-width fluctuations captured by M1 closely followed those measured by the reference system. Notably, the correlations remained stable even in turning, despite the increased medio-lateral variability characteristic of curved trajectories.

In contrast, M2 showed consistently poor agreement with the reference system. In straight walking, M2 yielded an RMSE of 9.2 cm—substantially worse than the 3.5 cm reported by Wang et al.—and performed even more poorly during turning, with an RMSE of 11.9 cm. Alongside these absolute errors, M2 produced extremely high MAE% values and very low Pearson correlations, with r remaining weak across all conditions. These findings suggest that, although M2 captured the approximate magnitude of stride width, it was unable to reflect meaningful step-to-step variations or respond reliably to changes in gait pattern, particularly during turning.

The discrepancy between ME and MAE% in M2 further highlights that the method performs poorly in relative terms: because stride width is a low-magnitude parameter, even modest absolute deviations generate disproportionately large percentage errors. Combined with the weak correlations, this indicates that M2 lacks the sensitivity required to track the medio-lateral adjustments of the gait cycle.

A likely explanation for M2's degraded performance compared with the results reported by Wang et al. lies in the different sensor configurations used. The original method was designed and trained for a shank-mounted IMU setup, whereas both M1 and M2 in this study were implemented using a foot-mounted configuration. Since machine-learning models strongly depend on the distribution of the training data and the kinematic characteristics of the sensor placement, applying Wang's model to a different mounting strategy introduces a mismatch that likely compromises prediction accuracy. By contrast, M1 was explicitly developed for the foot-mounted configuration adopted in this study, which may explain its comparatively better performance.

Despite the differences in sensor placement and training conditions between the two methods, the comparison conducted in this study remains highly informative. Very few methods currently exist that are capable of estimating stride width reliably outside controlled laboratory environments. This scarcity makes the comparative evaluation particularly valuable, as it provides rare insights into the behavior of different computational strategies applied to real-world gait analysis. Moreover, M2 represents the only openly accessible machine-learning approach for stride-width estimation available in the literature, with publicly released source code. This openness enabled a direct, transparent comparison between M1 and an established method from the state of the art—something that is seldom possible in gait-analysis research, where most algorithms remain proprietary or insufficiently documented. Thus, even though M2 was trained under different conditions, its inclusion provided an essential benchmark and offered meaningful context for interpreting the strengths and limitations of M1.

4.2 Advantages and limitations of the suggested method M1

The findings of this study highlight several advantages associated with the proposed method (M1) for estimating spatial gait parameters using foot-mounted inertial sensors.
A primary strength is its robust performance across diverse locomotor conditions, including straight and curvilinear walking and different self-selected gait speeds.

Unlike many IMU-based approaches that exhibit substantial performance degradation when gait deviates from steady, straight-line progression, M1 maintained consistent accuracy and correlation even during turning, a task known to introduce substantial variability in foot placement and medio-lateral control. This robustness underscores the method's suitability for real-world scenarios, where gait patterns are inherently non-linear and subject to continuous modulation.

Another key advantage of M1 is its capacity to estimate spatial gait parameters—including stride width—using only a single foot-mounted inertial sensor. This is particularly noteworthy, as stride width is rarely addressed in IMU-based studies despite its relevance to balance, stability, and fall risk [46]. The method demonstrated that accurate estimation of bilateral spatial parameters is achievable even with unilateral instrumentation.
By requiring only one sensor, M1 substantially reduces instrumentation burden, improves wearability, and simplifies both setup and deployment outside controlled laboratory settings. This minimal configuration enhances the feasibility of continuous gait monitoring in real-world environments while still providing reliable reconstruction of parameters that traditionally require bilateral sensing. This combination of simplicity and performance clearly distinguishes M1 from many existing methodologies.

However, this same feature introduces a notable trade-off. Because only one foot is directly instrumented, the contralateral side must be reconstructed indirectly. This unilateral sensing configuration can lead to asymmetries in the estimated parameters, particularly for those that depend heavily on bilateral foot-placement accuracy, such as step length and the Area of the Base of Support. While the method demonstrated generally stable performance, side-dependent discrepancies were nevertheless observed and may be further accentuated in more complex or variable walking conditions. Bilateral instrumentation would likely mitigate these effects and enhance the accuracy of parameters influenced by reconstruction uncertainty.

The method also benefits from being computationally lightweight, relying on deterministic algorithms rather than machine learning models. As a result, its performance is not dependent on training datasets, and it can be directly applied to new subjects or conditions without requiring model retraining or calibration procedures. This increases generalizability and facilitates clinical adoption.

Despite these advantages, several limitations must be acknowledged. Factors such

as uneven terrain, changes in footwear, or multitasking during walking were not assessed and may influence performance in real-world use.

Overall, while the method presents notable strengths in terms of robustness, simplicity, and ease of deployment—with the added advantage of requiring only a single foot-mounted sensor—its limitations indicate clear avenues for refinement, including bilateral instrumentation and evaluation across more diverse real-world conditions.

4.3 Clinical and practical implications

The methodological advances presented in this work have several important implications for both clinical practice and real-world gait analysis. First, the ability to reliably estimate spatial gait parameters—particularly stride width—using a single foot-mounted inertial sensor opens the possibility of lightweight, portable, and continuous gait monitoring. This represents a significant step toward integrating gait assessment into daily-life contexts, bridging the gap between laboratory-based measurements and ecological mobility evaluation.
Stride width is a parameter strongly associated with balance control, fall risk, and neurological conditions such as Parkinson's disease, cerebellar ataxia, and age-related gait instability [47]. A method capable of measuring this parameter accurately outside the laboratory could support early identification of deterioration in medio-lateral control and enable clinicians to detect subtle changes that may precede functional decline. Similarly, continuous monitoring of step length and AreaBoS provides a richer depiction of gait stability and can assist in evaluating rehabilitation progress, detecting compensatory strategies, or assessing the effectiveness of therapeutic interventions.
From a practical standpoint, the low computational cost and minimal instrumentation requirements of M1 facilitate large-scale deployment in clinical and research settings. The method can be integrated into wearable systems for remote monitoring, supporting telemedicine and home-based rehabilitation programs. Its robustness to walking-path variability also allows it to be applied during activities of daily living rather than being restricted to controlled clinical corridors.
The comparison with M2 further highlights the value of transparent and reproducible methodologies, which may be sensitive to training conditions and require large datasets for adaptation.

In summary, the proposed method holds considerable potential for improving gait analysis in both clinical and everyday environments, offering a practical, scalable, and robust tool for monitoring locomotor function and supporting data-driven

decision-making in rehabilitation and healthcare.

Chapter 5

Conclusion

The objective of this work was to evaluate the performance of an inertial-based method (M1) for estimating key spatial gait parameters, stride width, step length, and the Area of the Base of Support, during straight and curvilinear locomotion performed at different walking speeds. The method was assessed against a laboratory-grade reference system, and its performance was examined across multiple dimensions, including accuracy (ME, MAE%, RMSE), left–right parameter consistency, correlation with the reference, and robustness to changes in gait geometry. A second method from the literature (M2), based on machine learning and available as open-source code, was also tested to provide a comparative benchmark.
Across all analyses, M1 demonstrated reliable performance, with stable estimation of spatial parameters across speeds and path geometries. Stride width, in particular, showed the strongest agreement with the reference system, consistently yielding high correlations and moderate errors, even during turning tasks. Step length and AreaBoS exhibited more variability and side-dependent differences, partly attributable to the unilateral instrumentation of the sensing setup; nevertheless, M1 preserved overall consistency in both straight and curvilinear walking. Statistical analyses confirmed the method's stability, with no significant differences between straight and turning walking when right and left components were combined.
In contrast, M2 showed markedly lower performance, characterized by high relative errors and very weak correlations with the reference system across all conditions. Significant statistical differences emerged both between methods and between path types when analyzed with M2, indicating limited robustness to locomotor variability. These findings align with the methodological constraints of M2, which was trained using shank-mounted sensors—unlike the foot-mounted configuration used in this study—and was not trained on curvilinear gait. The mismatch between training conditions and experimental setup plausibly contributed to the poor generalization of M2.
Despite these limitations, the comparison remained valuable: few methods currently

exist for stride-width estimation outside the laboratory, and M2 represents the only open-source machine learning approach for this parameter, enabling a uniquely transparent and reproducible benchmark.

Overall, this study provides clear evidence that Method M1 offers a reliable and robust solution for estimating spatial gait parameters including stride with in real-world settings, including during curvilinear walking—the condition known to be particularly challenging for inertial systems. The work contributes novel quantitative insights into both straight and turning gait, expands the validation of base of support estimation methods beyond laboratory constraints, and highlights the importance of sensor placement and training data in model generalization.

Future work should consider incorporating bilateral instrumentation, which would improve symmetry in spatial estimation. Also expanding the population of this study to include pathological subjects may strengthen the validity of the method.

In conclusion, the present study demonstrates that inertial-based gait analysis, when supported by an appropriate processing framework, can provide accurate, stable, and reproducible estimation of key spatial parameters outside laboratory environments. Method M1 shows strong potential for applications in clinical assessment, rehabilitation monitoring, and longitudinal gait tracking in daily life scenarios.

Bibliography

[1] Jacquelin Perry and Judith M. Burnfield. *Gait Analysis: Normal and Pathological Function*. 2nd ed. Slack Incorporated, 2010 (cit. on pp. 4, 5, 8).

[2] Arnaldo Leal-Junior and Anselmo Frizera-Neto. «Optical Fiber Sensors for the Next Generation of Rehabilitation Robotics». In: (2022) (cit. on pp. 4, 6, 7).

[3] J. W. Gargano, M. J. Reeves, and Paul Coverdell National Acute Stroke Registry Michigan Prototype Investigators. «Sex differences in stroke recovery and stroke-specific quality of life: Results from a statewide stroke registry». In: *Stroke* 38.9 (2011), pp. 2541–2548. DOI: 10.1161/STROKEAHA.107.485482 (cit. on p. 4).

[4] W. Johnson, O. Onuma, M. Owolabi, and S. Sachdev. «Stroke: A global response is needed». In: *Bulletin of the World Health Organization* 94.9 (2016), 634–634A. DOI: 10.2471/BLT.16.181636 (cit. on p. 4).

[5] J. M. Hausdorff. «Gait dynamics in Parkinson's disease: Common and distinct behavior among stride length, gait variability, and fractal-like scaling». In: *Chaos: An Interdisciplinary Journal of Nonlinear Science* 19.2 (2009), p. 026113. DOI: 10.1063/1.3147408 (cit. on pp. 4, 22).

[6] M. E. Morris, R. Iansek, T. A. Matyas, and J. J. Summers. «Stride length regulation in Parkinson's disease. Normalization strategies and underlying mechanisms». In: *Brain* 119.2 (1996), pp. 551–568. DOI: 10.1093/brain/119.2.551 (cit. on p. 4).

[7] A. Mirelman, P. Bonato, and R. Camicioli. «Gait impairments in Parkinson's disease». In: *Handbook of Clinical Neurology*. Ed. by M. Hallett, L. R. Edwards, and J. M. Stone. Vol. 167. Elsevier, 2019, pp. 257–279. DOI: 10.1016/B978-0-12-804766-8.00015-1 (cit. on p. 4).

[8] Roberts. «Biomechanical parameters for gait analysis: a systematic review of healthy human gait». In: (2017) (cit. on p. 4).

[9] M. W. Whittle. *Gait analysis: An introduction*. 5th. Elsevier Health Sciences, 2014 (cit. on pp. 5, 8, 12).

[10] R. Baker. «Gait analysis methods in rehabilitation». In: *Journal of NeuroEngineering and Rehabilitation* 3.1 (2006), p. 4. DOI: 10.1186/1743-0003-3-4 (cit. on pp. 5, 10, 13).

[11] A. Muro-de-la-Herran, B. Garcia-Zapirain, and A. Mendez-Zorrilla. «Gait analysis methods: An overview of wearable and non-wearable systems, highlighting clinical applications». In: *Sensors* 14.2 (2014), pp. 3362–3394. DOI: 10.3390/s140203362 (cit. on pp. 5, 10).

[12] S. Lord, B. Galna, J. Verghese, S. Coleman, D. Burn, and L. Rochester. «Independent domains of gait in older adults and associated motor and nonmotor attributes: Validation of a factor analysis approach». In: *Journals of Gerontology Series A: Biological Sciences and Medical Sciences* 68.7 (2013), pp. 820–827. DOI: 10.1093/gerona/gls255 (cit. on p. 5).

[13] J. Hollman. «Normative spatiotemporal gait parameters in older adults». In: (2011) (cit. on p. 8).

[14] Christopher Vaughan. *Dynamics of Human Gait*. 2nd ed. 1992 (cit. on p. 9).

[15] A. Cappozzo and et al. «Human movement analysis using stereophotogrammetry. Part 1: theoretical background». In: *Gait & Posture* 21.2 (2005), pp. 186–196 (cit. on pp. 10–13, 21).

[16] S. Del Din and et al. «Free-living monitoring of Parkinson's disease: Lessons from the field». In: *Movement Disorders* 31.9 (2016), pp. 1293–1313 (cit. on p. 10).

[17] D. A. Winter. *Biomechanics and Motor Control of Human Movement*. 4th. Wiley, 2009 (cit. on pp. 13, 21).

[18] Christian Werner et al. «Assessing the Concurrent Validity of a Gait Analysis System Integrated into a Smart Walker in Older Adults with Gait Impairments». In: *Clinical Rehabilitation* (2019) (cit. on p. 13).

[19] Hylton B. Menz, Mark D. Latt, Anne Tiedemann, Belinda J. Munro, and Stephen R. Lord. «Reliability of the GAITRite® Walkway System for the Quantification of Temporo-Spatial Parameters of Gait in Young and Older People». In: *Gait & Posture* 20.1 (2003), pp. 63–68. DOI: 10.1016/S0966-6362(03)00068-7 (cit. on pp. 13, 21, 22).

[20] Guillaume Sacco et al. «Comparison of Spatio-Temporal Gait Parameters Between the GAITRite® Platinum Plus Classic and the GAITRite® CIRFACE Among Older Adults: A Retrospective Observational Study». In: *BMC* (2003) (cit. on p. 13).

[21] Jonas Johansson. «The Healthy Ageing Initiative: Prevention of Falls and Fractures». In: (Jan. 2018) (cit. on p. 14).

[22] P. Picerno. «25 years of lower limb joint kinematics by using inertial and magnetic sensors: A review of methodological approaches». In: *Gait & Posture* 51 (2017), pp. 239–246 (cit. on pp. 14, 18).

[23] Merryn J. Mathie, Branko G. Celler, Nigel H. Lovell, and Annet C. F. Coster. «Accelerometry: Providing an Integrated, Practical Method for Long-Term, Ambulatory Monitoring of Human Movement». In: *Physiological Measurement* 24.2 (2003), R1–R20. DOI: 10.1088/0967-3334/24/2/201 (cit. on p. 16).

[24] T. Seel, J. Raisch, and T. Schauer. «IMU-based joint angle measurement for gait analysis». In: *Sensors* 14.4 (2014), pp. 6891–6909 (cit. on p. 17).

[25] N. Yazdi, F. Ayazi, and K. Najafi. «Micromachined inertial sensors». In: *Proceedings of the IEEE* 86.8 (1998), pp. 1640–1659 (cit. on p. 18).

[26] A. M. Sabatini. «Estimating three-dimensional orientation of human body parts by inertial/magnetic sensing». In: *Sensors* 11.2 (2011), pp. 1489–1525 (cit. on pp. 18, 19).

[27] M. Mancini and F. B. Horak. «Potential of wearable sensors to improve balance assessment in clinical settings». In: *Movement Disorders* 26.9 (2011), pp. 1373–1383 (cit. on p. 19).

[28] Vıtor Miguel Santos et al. «A Systematic Review of Insole Sensor Technology: Recent Studies and Future Directions». In: *MDPI* (2024) (cit. on p. 20).

[29] Richard A. Brindle et al. «Validity of Estimating Center of Pressure During Walking and Running with Plantar Load from a Three-Sensor Wireless Insole». In: *Cambridge University Press* (2022) (cit. on p. 20).

[30] Pui Wah Kong et al. «Validation of In-Shoe Force Sensors During Loaded Walking in Military Personnel». In: *MDPI* (2023) (cit. on p. 20).

[31] Kristen E. Renner, Daniel B. Williams, and Robin M. Queen. «The Reliability and Validity of the Loadsol® Under Various Walking and Running Conditions». In: *Sensors* 19.3 (2019), p. 465. DOI: 10.3390/s19030465 (cit. on p. 20).

[32] Thomas Stöggl and Arno Martiner. «Validation of Moticon's OpenGo Sensor Insoles During Gait, Jump, Balance and Cross-Country Skiing Specific Imitation Movements». In: *Journal of Sports Sciences* 34.9 (2016), pp. 833–840. DOI: 10.1080/02640414.2015.1075050 (cit. on p. 20).

[33] Efthymios Ziagkas, Theodoros Pachidis, Maria Chatzipetrou, Ioannis Paraskevopoulos, Dimitrios Tsaopoulos, and Ioannis Kanellopoulos. «A Novel Tool for Gait Analysis: Validation Study of the Smart Insole PODOSmart®». In: *Sensors* 21.4 (2021), p. 1087. DOI: 10.3390/s21041087 (cit. on p. 21).

[34] Dirk Weenk et al. «Ambulatory Estimation of Relative Foot Positions by Fusing Ultrasound and Inertial Sensor Data». In: *IEEE*. 2015 (cit. on p. 22).

[35] Fokke B. van Meulen et al. «Ambulatory Assessment of Walking Balance After Stroke Using Instrumented Shoes». In: *Journal of NeuroEngineering and Rehabilitation* (2016) (cit. on p. 22).

[36] Nhat Hung Tran et al. «Inertial Sensor-Based Two Feet Motion Tracking for Gait Analysis». In: *Sensors* (2013) (cit. on p. 22).

[37] Tomas Bäcklund et al. «Novel, Clinically Applicable Method to Measure Step-Width During the Swing Phase of Gait». In: *IPEM*. 2020 (cit. on p. 22).

[38] Rachele Rossanigo et al. «Base of Support, Step Length and Stride Width Estimation During Walking Using an Inertial and Infrared Wearable System». In: *Sensors* (2023) (cit. on pp. 22, 23, 28, 34).

[39] Assaf Zadka et al. «A Wearable Sensor and Machine Learning Estimate Step Length in Older Adults and Patients with Neurological Disorders». In: *npj Digital Medicine* (2024) (cit. on p. 23).

[40] Julius Hannink et al. «Sensor-Based Gait Parameter Extraction With Deep Convolutional Neural Networks». In: (2017) (cit. on p. 23).

[41] H. Wang et al. «Step Width Estimation in Individuals With and Without Neurodegenerative Disease via a Novel Data-Augmentation Deep Learning Model and Minimal Wearable Inertial Sensors». In: *IEEE* (2024) (cit. on pp. 23, 26, 34, 37).

[42] Mohsen Sharifi Renani et al. «Deep Learning in Gait Parameter Prediction for OA and TKA Patients Wearing IMU Sensors». In: *Sensors* (2020) (cit. on p. 23).

[43] Stef Vandermeeren et al. «Feature Selection for Machine Learning Based Step Length Estimation Algorithms». In: *Sensors* (2019) (cit. on p. 23).

[44] S. Stančin and S. Tomažič. «Time- and Computation-Efficient Calibration of MEMS 3D Accelerometers and Gyroscopes». In: *Sensors* 14 (2014), pp. 14885–14915 (cit. on p. 28).

[45] D. Gebre-Egziabher, G.H. Elkaim, J. David Powell, and B.W. Parkinson. «Calibration of Strapdown Magnetometers in Magnetic Field Domain». In: *Journal of Aerospace Engineering* 19 (2006), pp. 87–102 (cit. on p. 28).

[46] Paul M. Riek et al. «Validation of Inertial Sensors to Evaluate Gait Stability». In: *Sensors* (2023) (cit. on p. 71).

[47] Ungbeom Kim et al. «Predicting Fall Risk Through Step Width Variability at Increased Gait Speed in Community-Dwelling Older Adults». In: *Scientific Reports* (2025) (cit. on p. 72).